Analysis of meiosis in *Pristionchus pacificus* reveals plasticity in homolog pairing and synapsis in the nematode lineage

Regina Rillo-Bohn[1,2*], Renzo S. Adilardi[1,2*], Therese Mitros[1], Bariş Avşaroğlu[1,2], Lewis Stevens[3], Simone Köhler[1,2 4], Joshua Bayes[1], Clara Wang[1,2], Sabrina Lin[1,2], K. Alienor Baskevitch[1,2], Daniel S. Rokhsar[1,5,6,7], and Abby F. Dernburg[1,2,8,9]

[1]Department of Molecular and Cell Biology, University of California, Berkeley, Berkeley, CA USA; [2]Howard Hughes Medical Institute, Chevy Chase, MD United States; [3]Darwin Tree of Life Project, Wellcome Sanger Institute, Cambridge, UK; [4]Present address: Cell Biology and Biophysics Unit, European Molecular Biology Laboratory, Heidelberg, Germany; [5]Department of Energy Joint Genome Institute, Berkeley, California 94720, USA. [6]Okinawa Institute of Science and Technology Graduate University, Onna, Okinawa 9040495; Japan, [7]Chan Zuckerberg Biohub, San Francisco, CA, USA [8]Biological Systems and Engineering Division, Lawrence Berkeley National Laboratory, Berkeley, CA USA, [9]California Institute for Quantitative Biosciences, Berkeley, CA USA

*Equal contribution

ABSTRACT

Meiosis is conserved across eukaryotes yet varies in the details of its execution. Here we describe a new comparative model system for molecular analysis of meiosis, the nematode *Pristionchus pacificus*, a distant relative of the widely studied model organism *Caenorhabditis elegans*. *P. pacificus* shares many anatomical and other features that facilitate analysis of meiosis in *C. elegans*. However, while *C. elegans* has lost the meiosis-specific recombinase Dmc1 and evolved a recombination-independent mechanism to synapse its chromosomes, *P. pacificus* expresses both DMC-1 and RAD-51. We find that SPO-11 and DMC-1 are required for stable homolog pairing, synapsis, and crossover formation, while RAD-51 is dispensable for these key meiotic processes. RAD-51 and DMC-1 localize sequentially to chromosomes during meiotic prophase and show nonoverlapping functions. We also present a new genetic map for *P. pacificus* that

reveals a crossover landscape very similar to that of *C. elegans*, despite marked divergence in the regulation of synapsis and crossing-over between these lineages.

INTRODUCTION

All sexually reproducing organisms rely on the specialized cell division process of meiosis to generate haploid gametes from diploid precursors. Upon fertilization, gametes fuse and restore the diploid chromosome complement in the zygote. This sexual cycle of meiosis and fertilization was likely present in the last eukaryotic common ancestor (Goodenough and Heitman, 2014). Studies in plants, animals, fungi, and protists have revealed intriguing diversity in the details of meiotic mechanisms.

A defining feature of meiosis is a “reductional” segregation in which homologous chromosomes are separated, usually during the first of two nuclear divisions. A highly choreographed series of chromosome transactions precedes this division and ensures faithful homolog segregation: (1) pairing, in which chromosomes contact and recognize their homologous partners; (2) synapsis, defined as the assembly of a protein ensemble called the synaptonemal complex (SC) between homologs, which stabilizes pairing and leads to their lengthwise alignment; and (3) crossover (CO) recombination, which creates physical links between chromosomes that promote proper bi-orientation during anaphase I. Failure to form at least one “obligate” CO between each pair of homologs typically results in missegregation and aneuploid gametes (Zickler and Kleckner, 2015).

Although homolog pairing, synapsis and CO recombination during meiosis are nearly ubiquitous among eukaryotes, key aspects of these chromosomal transactions show remarkable diversity across different lineages. In most model fungi, plants, and

animals, synapsis is thought to be triggered by early steps in recombination. Meiotic recombination is initiated by double-strand breaks (DSBs) catalyzed by the conserved topoisomerase-like enzyme Spo11 (Bergerat et al., 1997; Keeney et al., 1997). DSBs are resected to form 3' single-stranded DNA overhangs. Dmc1, a meiosis-specific recombinase, forms filaments along the resulting ssDNA segments and promotes interhomolog strand invasion to form joint molecules (JMs). Rad51 is often required as a cofactor for Dmc1. A subset of these JMs is ultimately repaired through a meiosis-specific pathway that generates COs, while the rest are mostly repaired through a more "mitotic-like" homologous recombination pathway to yield non-CO products (Hunter, 2015; Kohl and Sekelsky, 2013).

Spo11-dependent induction of DSBs and Dmc1-dependent strand invasion are crucial for synapsis, and thus for stable homolog pairing, in the budding yeast *Saccharomyces cerevisiae*, the flowering plant *Arabidopsis thaliana,* and in mice (Bishop et al., 1992; Couteau et al., 1999; Grelon, 2001; Pittman et al., 1998; Rockmill et al., 1995; Yoshida et al., 1998). Thus, the formation of JMs is considered to be an intrinsic part of the pairing process by which chromosomes recognize their partners. In contrast, recombination-independent mechanisms of pairing and synapsis have been characterized in other prominent model systems, including the dipteran insect *Drosophila melanogaster* and the nematode *Caenorhabditis elegans* (Lake and Hawley, 2012; Rog and Dernburg, 2013). While crossing-over is essential for successful execution of meiosis in *C. elegans* and in female fruit flies, homolog pairing and synapsis can be uncoupled from DSB formation and JM formation. In *Drosophila melanogaster* females, pairing initiates in proliferating germline cells even before they

enter meiosis and is stabilized by SC formation during early prophase (Christophorou et al., 2015, 2013). *D. melanogaster* males lack both recombination and SCs and have apparently evolved a distinct mechanism to stabilize homolog pairing and enable reductional segregation (McKee et al., 2012). In *C. elegans*, pairing and synapsis are both mediated by Pairing Centers (PCs), specialized sites on each chromosome bound by a family of zinc-finger proteins that interact with nuclear envelope proteins and promote large-scale chromosome movement (MacQueen et al., 2005; Phillips et al., 2005; Phillips and Dernburg, 2006; Sato et al., 2009). While interactions between chromosomes and nuclear envelope proteins play important roles in meiotic pairing and synapsis across eukaryotes, in *C. elegans* they have acquired a critical role in coupling homolog pairing to synapsis initiation (Penkner et al., 2007, 2009; Sato et al., 2009).

To investigate how the meiotic program is modified during evolution, we have established tools to investigate meiosis in the free-living nematode *Pristionchus pacificus,* which has been established as a model for studies in development, evolution and ecology (Sommer, 2015). Like its distant relative *C. elegans*, *P. pacificus* is an androdioecious species, with populations consisting of self-fertilizing hermaphrodites (XX) and a low frequency of spontaneous males (XO) (Sommer, 2015; Sommer et al., 1996). *P. pacificus* also shares with *C. elegans* a short life cycle of 3.5 days at 20˚C, produces large broods of about 200 progeny by self-fertilization, and is easily cultured in the lab (Hong and Sommer, 2006). Although *C. elegans* and *P. pacificus* diverged an estimated 60-90 million years ago (Werner et al., 2018), they share the same number of chromosomes (2n=12). Other than one major chromosomal translocation, macrosynteny is largely maintained between the two species (Dieterich et al., 2008;

Rödelsperger et al., 2017) as well as other Rhabditids. Like other nematodes, *P. pacificus* is thought to have holocentric chromosomes, which we confirm here through cytological analysis. Recent improvements in the genome assembly (Rödelsperger et al., 2017) and advances in genome editing (Lo et al., 2013; Namai and Sugimoto, 2018; Witte et al., 2015) have facilitated investigation of developmental and cell biological processes at a more mechanistic level.

We became interested in exploring meiosis in *P. pacificus* in part because of differences in the inventory of meiotic genes predicted from its genome sequence compared to *C. elegans.* In particular, genome sequencing and annotation have revealed the presence of genes encoding an ortholog of Dmc1 as well as two Dmc1 cofactors, Mnd1 and Hop2, all of which are absent from the entire *Caenorhabditis* clade (Figure 2 - Supplement 1 and (Dieterich et al., 2008)). Loss of Dmc1 correlates with the adaptation of recombination-independent mechanisms for pairing and synapsis in *Drosophila* and *Caenorhabditis* (Villeneuve and Hillers, 2001). Therefore, we were keen to examine how homologous chromosomes pair and synapse in *P. pacificus*. In addition, genetic linkage maps have suggested that multiple COs typically occur per chromosome pair during meiosis in *P. pacificus* (Hong and Sommer, 2006; Srinivasan et al., 2003, 2002), while only a single crossover per chromosome pair normally occurs during meiosis in *C. elegans*, suggesting potential differences in crossover regulation.

Using genome editing, cytogenetic analysis, and recombination mapping, we have characterized the early events of meiotic prophase in *P. pacificus*. We show that homolog pairing, synapsis and CO recombination are dependent on *Ppa-spo-11* and *Ppa-dmc-1*, while *Ppa-rad-51* is not essential for meiosis. We find that crossover sites

are designated very early during meiotic prophase, prior to completion of synapsis, and are limited to one per chromosome pair. We also present a new genetic map, which corroborates our cytological evidence that a single crossover normally occurs between each pair of homologs per meiosis in in both spermatocytes and oocytes. The map also provides evidence of crossover suppression and segregation distortion of specific chromosomes in hybrids, indicative of reproductive barriers between strains. Our work highlights both conserved and flexible features of the meiotic program within the nematode lineage and establishes a platform for future investigation.

RESULTS

P. pacificus as a comparative model system for meiosis

The morphology and organization of the *P. pacificus* germline is very similar to that of *C. elegans*. Hermaphrodites have two tubelike gonad arms in which sperm and ova are produced sequentially, while males have a single arm (Rudel et al., 2005). These are organized as a cylindrical monolayer of cells abutting a central core, or rachis. The distal tip is populated by proliferating germline stem cells (Figure 1A, B, D), as confirmed by the incorporation of microinjected fluorescently labeled nucleotides into replicating DNA (Figure 1B). As in *C. elegans*, meiotic entry is marked by an obvious change in nuclear organization in which fluorescently-stained chromosomes form a conspicuous crescent-shaped mass (Figure 1A). Immediately proximal to this “transition zone,” DAPI staining reveals parallel tracks, indicative of paired and synapsed homologous chromosomes at the pachytene stage. Gametogenesis switches from spermatogenesis to oogenesis occurs during early adulthood. As oocytes approach

maturation, chromosomes undergo striking decondensation between diplotene and diakinesis, a stage that has been referred to as the “growth zone” (Rudel et al., 2005). Similar chromosome morphology is observed during a late “diffuse stage” of meiotic prophase in many other eukaryotes (Zickler and Kleckner, 1999), but is rarely seen in *C. elegans*. In the most proximal region of the hermaphrodite gonad, oocytes mature and form a single row of large cells, and chromosomes condense dramatically as the nuclei grow in size. Six bivalents can be detected as compact DAPI-staining bodies in oocytes at diakinesis, the last stage of meiotic prophase preceding the first meiotic division (Figure 1A, C, Rudel et al., 2005; Sommer et al., 1996).

It has been assumed that chromosomes in *P. pacificus* are holocentric, as in *C. elegans*, but we are unaware of direct evidence to support this idea. We thus identified a gene encoding CENP-C (HCP-4 in *C. elegans*), a conserved kinetochore protein, in the *P. pacificus* genome and inserted a V5 epitope tag at its 3’ end. The distribution of CENP-C on mitotic chromosomes in embryos and mitotic germ cells confirmed their holocentric organization (Figure 1D). Kinetochores appeared as linear structures along the full length of chromosomes, rather than discrete foci. CENP-C also coated the chromosomes during meiotic metaphase I (Figure 1C), as in *C. elegans* (Shakes et al., 2009).

Stable homolog pairing requires early recombination factors

BLAST searches of the *P. pacificus* genome revealed an open reading frame encoding an unambiguous ortholog of Dmc1, a meiosis-specific paralog of Rad51 (Table S1). Orthologs of the Dmc1 cofactors Mnd1 and Hop2 were also identified by

homology searches (Figure 2 – Supplement 1). By contrast, Dmc1/Mnd1/Hop2 are absent from both *C. elegans* and *D. melanogaster*, two model organisms that have evolved recombination-independent mechanisms of homolog pairing and synapsis (Villeneuve and Hillers, 2001). We analyzed the genome sequences of other nematodes to determine the evolutionary history of these genes within the nematode lineage. This analysis revealed that Dmc1/Mnd1/Hop2 have been lost several times during the evolution of nematodes, including the entire *Caenorhabditis* genus and all sequenced members of Clade IV (Figure 2 –Supplement 1). As expected in light of its essential function in DNA repair, the recombinase Rad51 was detected in all genomes examined (data not shown).

In *C. elegans*, homolog pairing and synapsis require a family of zinc-finger proteins (HIM-8, ZIM-1, ZIM-2, and ZIM-3) that bind to motifs enriched within Pairing Center (PC) regions near one end of each chromosome (Phillips et al., 2009b). We identified homologs of these proteins in many of the genome sequences from Clade V nematodes, but not in *Pristionchus*. Because these homologs are present in species that retain intact DMC-1 genes, it is unlikely that PC proteins arose as an alternative to DMC-1 function in meiosis, although in *Caenorhabditis* they may have acquired a role that eventually allowed degeneration and loss of DMC-1.

We tested whether homolog pairing in *P. pacificus* depends on double-strand breaks or strand-exchange proteins. To generate *spo-11, dmc-1* and *rad-51* null mutants, we first employed TALEN-mediated gene disruption, and later CRISPR/Cas9 genome editing techniques (this study; Lo et al., 2013; Witte et al., 2015). Genome editing has thus far been less efficient in *P. pacificus* than in *C. elegans*, and techniques

such as co-CRISPR (in which another locus is edited to an allele with a visible phenotype) have not been helpful to enrich for the desired edited progeny in our hands or others' (Witte et al., 2015, and data not shown). Nevertheless, we were readily able to isolate mutant alleles by screening a large number of F1 progeny from injected hermaphrodites (see Materials and Methods). Independent alleles isolated from either TALEN- or CRISPR-mediated genome editing resulted in identical mutant phenotypes. All data presented here were based on alleles generated by CRISPR/Cas9. Because balancer chromosomes are not currently available for *P. pacificus*, most mutations described here were maintained in unbalanced heterozygotes, with frequent PCR-based genotyping. Self-fertilization of heterozygotes results in broods with 25% homozygous mutant animals, which were identified based on their phenotype and/or immunostaining to determine the presence or absence of the protein of interest. We also found that a freezing method developed for *C. elegans* that uses DMSO and trehalose as cryoprotectants (Kevin F. O'Connell, Worm Breeders' Gazette, pers. comm.) allowed robust recovery of frozen *P. pacificus*, facilitating strain maintenance and archival storage.

As expected, disruption of either *spo-11* or *dmc-1* resulted in the detection of 12 DAPI-staining univalent chromosomes at diakinesis, indicative of a failure in CO recombination (Figure 5). Surprisingly, *rad-51* mutants were fertile and displayed only mild meiotic defects (see below). We thus validated the loss of RAD-51 function in mutant animals by generating multiple alleles, which showed indistinguishable phenotypes. We also confirmed the absence of RAD-51 protein by immunofluorescence with a polyclonal antibody raised against recombinant Ppa-RAD-51 (Figure 4 –

Supplement 1B, see Materials and Methods). Mutations in *spo-11* or *dmc-1,* but not *rad-51,* resulted in an obvious extension of the region of the germline displaying the crescent-shaped nuclear morphology characteristic of early meiosis (Figure 2 – Supplement 2). A similar “extended transition zone” phenotype is seen in *C. elegans* mutants that fail to synapse their chromosomes during meiosis, suggesting that *spo-11* and *dmc-1* might be required for synapsis in *P. pacificus*.

To visualize and quantify homolog pairing, we generated FISH probes against two short tandem repeats found on Chromosomes X and IV (Figure 2A). We measured the distance between pairs of homologous FISH signals in individual nuclei for each genotype. To analyze pairing kinetics, we divided the distal gonads into five zones of equal length. In zone 1, which contains mostly proliferating germ cells, pairs of FISH signals remained far apart, with an average distance of 2.4 ± 1.0 μm (SD) and 2.5 ± 0.8 μm for Chromosomes X and IV, respectively (Figure 2B, D). In zone 2, which spans the transition zone, the average distances decreased significantly in wild-type animals (1.2 ± 1.1 μm and 1.1 ± 1.1 μm for probes on Chromosomes X and IV, respectively), and homologous signals remained closely associated in the subsequent meiotic stages. Notably, homologous FISH probes localized closer together, on average, in the two zones immediately following meiotic entry, and showed some separation in zones 4 and 5 (Figure 2B, D). By contrast, in wild-type *C. elegans*, homologous loci remain closely apposed in most throughout an extended pachytene stage spanning most of the distal region (before the “loop”) of the gonad (MacQueen, 2002). Together with analysis of synapsis (below), this indicated that desynapsis initiates soon after completion of synapsis in *P. pacificus*, resulting in partial separation of homologs.

We noted that the average distances between pairs of homologous FISH signals in *spo-11* and *dmc-1* mutants also decreased markedly upon meiotic entry, although clearly less so than in wild type (Figure 2D). In contrast, *rad-51* mutants showed distributions of probe distances more similar to wild-type animals (Figure 2C, D). We considered the possibility that the proximity between FISH signals might reflect the clustering of all chromosomes during leptotene/zygotene, rather than specific homologous interactions. If so, the extended transition zone morphology in *spo-11* and *dmc-1* might obscure a pairing defect that would be more apparent in the absence of clustering (Figure 2 – Supplement 2). To address this, we measured the distances between pairs of heterologous FISH signals in the premeiotic region (dispersed) versus the transition zone (clustered). We observed that FISH signals on different chromosomes were also significantly closer to each other in the transition zone compared to premeiotic nuclei in both wild-type and mutant animals (Figure 2E). The distances between heterologous versus homologous pairs of FISH loci were not significantly different in *spo-11* and *dmc-1* mutants ($p=0.1777$ and $p=0.6774$, respectively, by Student's *t*-test), but homologous signals were clearly closer than heterologous signals in wild-type meiocytes ($p<0.0001$ by Student's *t*-test) (Figure 2E). These data support the idea that clustering, rather than specific pairing, promote proximity between both homologous and heterologous loci during leptotene/zygotene in *spo-11* and *dmc-1* mutants. Although we cannot conclude that transient homologous pairing is absent in these mutants, it is evident that these early recombination factors are required for stable pairing and extended association of homologous loci throughout prophase. In contrast, *rad-51* is dispensable for homolog pairing, as in *C. elegans*.

SPO-11 and DMC-1 are required for homologous synapsis

To further investigate meiotic progression in *P. pacificus* and to probe the role of early recombination factors in synapsis, we developed cytological markers for the chromosome axis, which normally assembles upon meiotic entry, and the synaptonemal complex (SC), which assembles between paired axes during early prophase. Identification of a candidate axial element component was straightforward, due to the presence of the easily recognized HORMA (Hop1, Rev7, Mad2) domain among members of this family of proteins (Aravind and Koonin, 1998; Vader and Musacchio, 2014). We identified a gene encoding a HORMA domain protein that is most closely related to *C. elegans* HIM-3 by reciprocal BLAST analysis (Table S1). We refer to this protein as Ppa-HOP-1, after the founding member of the meiotic HORMA proteins, *S. cerevisiae* Hop1 (Hollingsworth and Byers, 1989, p. 1). Using genetic immunization, we raised a polyclonal antibody against a 100-amino acid segment of the predicted protein including part of the HORMA domain and found that it indeed recognized chromosome axes from meiotic entry through late prophase (Figure 3A, B).

To enable cytological detection of synaptonemal complex (SC) assembly, we searched for homologs of SC proteins. This was not straightforward due to rapid divergence of these proteins in nematodes as well as their extensive regions of coiled-coil potential, which is associated with a strongly skewed amino acid composition. *C. elegans* expresses six known SC proteins, known as SYP-1–6. SYP-4 has a distinctive C-terminal domain containing several unusual motifs enriched in glycine and phenylalanine residues. We generated and sequenced an RNA library from isolated

gonads, which facilitated identification of full-length *Ppa-syp-4.* We inserted an HA epitope tag at the C-terminus of the endogenous coding sequence, and found that immunofluorescence with an epitope-specific antibody localized specifically between paired meiotic chromosomes, confirming SYP-4::HA as a marker for the SC (Figure 3A, B). The tagged protein supported normal meiosis, as indicated by the low percentage of inviable embryos and males in the strain population (Figure 3 – Supplement 1).

HOP-1 was detected in the nucleoplasm in the premeiotic region of the germline and formed linear structures along chromosomes upon meiotic entry. SYP-4 was detected along chromosome segments shortly thereafter, and fully colocalized with HOP-1 tracks during pachytene. Notably, the region of the germline containing nuclei with fully aligned stretches of SYP-4 and HOP-1 was very short compared to *C. elegans,* in which SC disassembly occurs close to the bend of the gonad arm, shortly prior to diakinesis. In contrast, SC disassembly initiated much earlier in *P. pacificus*; the major fraction of prophase nuclei are thus arrested at diplotene, since chromosomes are only partially synapsed. Six short stretches of SYP-4 were apparent in these nuclei, which persisted over an extended region (Figure 3A, B). This asymmetrical pattern of SC disassembly is highly reminiscent of a more transient diplotene stage in *C. elegans*, in which the SC remains associated with one “arm” of each homolog pair and subsequently contributes to the step-wise loss of cohesion during the meiotic divisions (Cloud et al., 2012; Da Ines et al., 2013).

HOP-1 localized normally to chromosome axes in *spo-11* and *dmc-1* mutants, but extensive SC assembly failed. Instead, small, dispersed puncta of SYP-4 were observed along chromosome axes, with occasional longer tracks (Figure 3C). In

contrast to *spo-11* and *dmc-1* mutants, *rad-51* mutants displayed robust synapsis with a distribution of stages similar to that seen in wild-type hermaphrodites (Figure 3C). These observations indicate that homologous synapsis depends on SPO-11 and DMC-1 in *P. pacificus*, in contrast to the recombination-independent synapsis seen in *C. elegans*.

DMC-1 and RAD-51 localize sequentially during distinct stages of meiotic prophase

To investigate the functions of and interplay between DMC-1 and RAD-51 in *P. pacificus*, we inserted a V5 epitope tag at the C-terminus of DMC-1 using CRISPR/Cas9 and raised a polyclonal antibody that recognizes RAD-51 (see Materials and Methods). DMC-1::V5 supported normal meiosis, as evidenced by a normal brood size, high embryonic viability and low percentage of males (Figure 3 – Supplement 1). Surprisingly, the two proteins showed distinct and nonoverlapping patterns of localization. DMC-1 localized very broadly along chromosomes, in transition zone nuclei and disappeared immediately upon completion of synapsis. RAD-51 displayed a much more restricted, punctate distribution along chromosomes, which was only detected in nuclei in which DMC-1 no longer coated the chromosomes (Figure 4A, B). Occasional nuclei at the border between the transition zone and pachytene region exhibited both DMC-1 and RAD-51, although DMC-1 was very faint in these nuclei and did not overlap with RAD-51 (Figure 4C). Additionally, DMC-1 remained strongly associated with chromosomes in some late nuclei that retained clustered DAPI morphology, presumably either “straggler” nuclei with delays in synapsis or CO designation, or apoptotic cells,

both of which are typically observed in the germlines of wild-type *C. elegans* (Figure 4D). Differences between the localization of DMC-1 and RAD-51 were further validated by inserting a V5 epitope tag at the C-terminus of RAD-51. Staining of this strain with anti-V5 recapitulated the sparse, punctate localization seen with anti-RAD-51 antibodies, demonstrating that the broader distribution of DMC-1 is not an artifact of the V5 epitope tag or antibody (Figure 4 – Supplement 1A). RAD-51::V5 also supported normal meiosis, with a normal brood size, high embryonic viability and low frequency of male self-progeny (Figure 3 – Supplement 1).

We also tested the interdependence of DMC-1 and RAD-51 recombinases for their localization. In *S. cerevisiae* and *A. thaliana*, Dmc1 functions as an essential catalyst for interhomolog joint molecule (JM) formation during meiotic DSB repair, while Rad51 acts as an accessory protein for Dmc1 nucleofilament formation (Cloud et al., 2012; Da Ines et al., 2013). We did not detect RAD-51 in transition zone nuclei, where DMC-1 was abundant on chromatin, and we found that DMC-1::V5 localization was normal in *rad-51* mutants, indicating that RAD-51 does not play an essential role in the recruitment of DMC-1 (Figure 4 – Supplement 1B). Conversely, in *dmc-1* mutants we detected RAD-51 foci only in late prophase nuclei, proximal to the very extended transition zone (Figure 4 – Supplement 1C). RAD-51 foci were more abundant and larger in *dmc-1* mutants than in wild-type pachytene nuclei, perhaps due to persistent unrepaired DSBs that accumulate in the absence of DMC-1 protein. Alternatively, the bright foci of RAD-51 observed in late prophase nuclei could reflect an apoptotic response to unrepaired breaks and/or extensive asynapsis.

The number of DMC-1 foci could not be quantified meaningfully due to their density and wide variation in intensity, but the broad distribution suggests that DMC-1 associates with intact dsDNA in addition to sites undergoing recombination. Nevertheless, in *spo-11* mutants DMC-1 was restricted to one or a few nuclear aggregates rather than broadly along chromosomes (Figure 4 – Supplement 1D). It was unclear whether these were associated with chromatin. This mislocalization may reflect either an absence of potential binding sites due to an absence of DSBs, or *spo-11*-dependent regulation of DMC-1 binding to chromatin, perhaps through activation of a DNA damage signaling pathway.

In contrast, RAD-51 foci are much sparser along chromosomes, suggesting that the protein localizes specifically to recombination intermediates. Thus, it was unsurprising to see that RAD-51 foci were absent from meiotic nuclei in *spo-11* mutants (Figure 4 – Supplement 1F). Some RAD-51 foci were observed in the mitotically proliferating region the germline in *spo-11* mutants, as in wild-type animals, providing a positive control for immunofluorescence (Figure 4 – Supplement 1E).

Together these observations indicate that DMC-1 and RAD-51 bind to chromatin at distinct stages of meiotic prophase and are not interdependent, although both require DSBs for their localization to chromosomes.

RAD-51 is not required for CO formation or completion of meiosis

To assess the roles of DMC-1 and RAD-51 in CO formation, we quantified the number of DAPI-staining bodies at diakinesis in *dmc-1* and *rad-51* mutants. Wild-type oocytes at this stage usually have six bivalents that can be resolved as discrete DAPI-

staining bodies (average = 5.6), while in *spo-11* mutants, ~12 DAPI-staining bodies were detected (average= 11.5), consistent with an absence of COs (Figure 5A, B). Interestingly, we frequently failed to detect oocytes at diakinesis in *dmc-1* mutant germlines, indicative of a defect in meiotic progression and the likely activation of a checkpoint in response to unrepaired DSBs. In cases when we did see nuclei at diakinesis, we observed an average of 11.6 DAPI-staining bodies, reflecting an absence of COs, as in *spo-11* mutants (Figure 5A-C).

Unexpectedly, disruption of *rad-51* resulted in homozygous mutant hermaphrodites that were viable and fertile, although animals produced smaller broods and their embryos showed greatly reduced viability (Figure 5D). This was surprising because RAD-51 is essential for completion of meiosis in most organisms where it has been examined. Homozygous *rad-51* mutant gonads also displayed diakinesis nuclei more frequently than *dmc-1* mutants, although they were absent in 2 out of 20 gonads scored, indicating that loss of DMC-1 function impairs meiotic progression more severely than loss of RAD-51 (Figure 5C). Consistent with this observation, while self-fertilizing *rad-51* mutants had a lower average brood size than wild-type hermaphrodites, *dmc-1* mutants had even smaller broods, ranging from zero to 35 embryos laid per mutant homozygote (Figure 5D). In striking contrast to *C. elegans rad-51* mutants, which display chromatin aggregates and fragments at diakinesis (Martin et al., 2005; Rinaldo et al., 2002), *Ppa-rad-51* mutants displayed an average of 6 DAPI-staining bodies, similar to wild-type (Figure 5B). Together with the relatively high viability of progeny of *rad-51* homozygous mutants, this indicates that RAD-51 does not play an essential role in CO formation in *P. pacificus.*

COSA-1 marks designated CO sites during throughout early prophase

To further analyze CO formation in *P. pacificus*, we identified the gene encoding the metazoan meiotic cyclin-related protein COSA-1 (Crossover Site Associated) /Cntd1 (Cyclin N-terminal Domain Homology) and inserted a 3xFLAG epitope tag at the C-terminus of the coding sequence. The strain expressing COSA-1::3xFLAG yielded progeny with high embryonic viability and few males, indicating that the tagged protein supports normal meiosis (Figure 3 – Supplement 1). Immunostaining with anti-FLAG antibodies revealed discrete foci along the SC, beginning as early as zygotene, which decreased in number and became brighter within the short pachytene region (Figure 6A, B). Most pachytene nuclei displayed 6 COSA-1 foci, each of which was associated with an individual SC, indicating the presence of a single designated crossover site between each pair of homologs (Figure 6C and Supplemental Video 1). We stained J4 larval-stage hermaphrodites whose germlines had not yet undergone the switch from spermatogenesis to oogenesis and found that pachytene spermatocytes also displayed ~6 COSA-1 foci (Figure 6- Supplemental Figure 1A). This suggests that *P. pacificus*, like *C. elegans*, has robust chromosome-wide CO interference in both spermatogenesis and oogenesis.

Intriguingly, SC disassembly appeared to be regulated by the position of the designated CO site, as in *C. elegans.* By mid-prophase, 6 short stretches of SYP-4::HA were observed, each associated with a single COSA-1::3xFLAG focus near one end (Figure 6B). As meiosis progressed further, COSA-1::3xFLAG foci became undetectable, although short stretches of SYP-4::HA could still be observed. We also

observed splaying of chromosome axes along the “long arms” on one side of the COSA-1 focus upon disappearance of the SC from those regions (Figure 6D). HOP-1 was retained on both arms following SC disassembly, although the signal appeared fainter along the long arms, perhaps due to separation of the two axes. At this stage, short stretches of SYP-4::HA colocalize with corresponding bright stretches of HOP-1 (Figure 3B and Figure 6D). Bivalents at diakinesis and meiotic metaphase I also displayed a cruciform structure similar to that seen in *C. elegans*, consistent with a single chiasma per chromosome pair (Figure 1C).

In *C. elegans* the orientation of chromosomes during meiotic segregation is stochastically determined by the position of the single crossover between each pair: the “long arm,” where SC first disassembles, is designated to retain cohesion and to lead towards the poles while the “short arm” releases cohesion during MI, but then becomes the leading end for segregation of chromatids during meiosis II (Albertson and Thomson, 1993). Using FISH to mark specific chromosome regions together with immunostaining of SYP-4::HA, we found that the same was true for *P. pacificus*: an asymmetrically localized probe localized to either the long (desynapsed) arm or the short arm in different nuclei (Figure 6- Supplemental Figure 2).

We examined the localization of COSA-1::3xFLAG in various mutant backgrounds. As expected, *dmc-1* mutants showed a complete absence of COSA-1 foci throughout prophase, while 6 foci were observed in pachytene nuclei in *rad-51* mutants (Figure 7A), consistent with the number of DAPI-staining bodies observed at diakinesis in these mutants (Figure 5B). A few bright COSA-1::3xFLAG foci were present throughout prophase in *spo-11* mutants (Figure 7A). However, since ~12 DAPI-staining

bodies were observed during diakinesis, we conclude that these COSA-1 foci do not mark designated COs. A similar phenomenon has been reported in C. elegans *spo-11* mutants (Nadarajan et al., 2017; Pattabiraman et al., 2017), suggesting that COSA-1 and other crossover factors can coalesce at sites lacking bona fide recombination intermediates when such structures are absent.

A genetic map for *P. pacificus* reveals conservation of the CO landscape

Prior work has led to divergent estimates of the meiotic recombination frequency in *P. pacificus*. By summing over measured genetic intervals on the same linkage group, the Sommer lab initially concluded that the map length of each chromosome exceeded 100 cM, with a maximum length of 215 cM for Chromosome I, which is also physically the longest (Hong and Sommer, 2006; Srinivasan et al., 2003, 2002). However, a map derived by the same group based on RNA sequencing of ~F10 Recombinant Inbred Lines (RILs) yielded markedly shorter genetic lengths, below 100 cM per chromosome (Rödelsperger et al., 2017).

Since an understanding of the crossover landscape is an important reference for analysis of meiosis, we addressed this ambiguity by constructing a new genetic map for *P. pacificus*. We used three divergent parental strains from different geographic regions: PS312 from California (CA), PS1843 from Washington State (WA), and RSB001 from La Réunion island (LR) and mated them using a double-cross hybrid strategy. A total of 93 progeny from a cross between CA/WA hybrid males and CA/LR hybrid hermaphrodites were sequenced (Figure 8A). This strategy allowed us to

simultaneously map crossovers that occur during hermaphrodite oogenesis and male spermatogenesis from the same progeny (Figure 8B).

We draw several conclusions from the resulting crossover maps (Figure 8C). First, the map lengths for each chromosome are close to 50 cM for both oocyte and spermatocyte meiosis, very similar to genetic map lengths in *C. elegans*. This indicates that a single crossover usually occurs between each pair of chromosomes per meiosis, consistent with our cytological observations. Close to half of all chromatids inherited from either parent are non-recombinant, as expected if a single crossover occurs between two of the four possible chromatids. We did observe a few examples of double crossovers in our data, but such events are rare (6/1012 chromatids). Second, the distal regions ("arms") show higher recombination rates than the central regions of each chromosome, as in *Caenorhabditids* (Barnes et al., 1995, Rockman and Kruglyak, 2009). This bias was also evident in a map constructed using RNA sequencing data (Rödelsperger et al., 2017) and seems to be a widely conserved feature among Rhabditids and perhaps other nematode clades (Doyle et al., 2018, Gonzalez de la Rosa et al., 2021).

Third, the male spermatocyte map showed a pronounced asymmetry for Chromosomes III and IV, with COs occurring predominantly on one arm, whereas the corresponding oocyte maps show COs on both arms. Conversely, the oocyte-specific map for the X chromosome shows an absence of crossovers on the right arm (the single X chromosome does not undergo COs during male spermatogenesis) (Figure 8C). These findings suggest that crossovers were suppressed on one side of these chromosomes in the hybrid parents. This suppression may reflect structural

rearrangements between the parental strains. Specifically, there are likely structural differences between the Washington and California versions of Chromosomes III and IV, and between the La Réunion and California versions of the X chromosome. A lack of crossovers on the right arm of the X chromosome is also evident in data from RILs from a cross between the same strains from La Réunion and California (Rödelsperger et al., 2017). Crossover suppression on Chromosomes III and IV likely reflects intra- rather than inter-chromosomal rearrangements, since we do not see evidence for pseudolinkage, as would be expected if a III; IV translocation were present. Notably, the asymmetry in crossover suppression also suggests that one arm of each chromosome may contain a region that plays a dominant role in homolog pairing during meiosis, perhaps related to the function of PCs in *C. elegans* (see discussion for more details). This was unexpected given the absence of obvious orthologs of the zinc finger proteins required for PC function in *C. elegans*, and the more “conventional” dependence of pairing and synapsis on recombination that we have documented for *P. pacificus*.

Finally, we detected pronounced segregation distortion for chromosomes I and II in the oocyte map, with inheritance of the La Réunion haplotype strongly favored (Figure 8 – Supplement 1B). In each case non-recombinant chromosomes of the La Reunion haplotype were about 8-fold more frequently inherited than the non-recombinant California chromatids. These observations are consistent with either a bias in meiosis segregation -- i.e., meiotic drive -- or the presence of loci on these chromosomes that cause genetic incompatibilities (i.e., inviability of some F2 progeny). Analysis of recombinant chromatids suggests that the latter scenario is more likely, since a gradient in the severity of the distortion can be detected along the physical

length of the chromosomes, consistent with the idea that specific loci on the affected autosomes may be toxic to hybrid progeny.

DISCUSSION

Distinct roles for DMC-1 and RAD-51

Comparison of the activities of Rad51 and Dmc1 *in vitro* has revealed similar profiles: both RecA homologs bind preferentailly to single-stranded DNA and can mediate strand-exchange interactions. However, Dmc1 is uniquely required during meiosis. The distinct requirements for Rad51 and Dmc1 are thought to be due in part to the activity of Dmc1 specific cofactors Mnd1 and Hop2, which confer different activities, and/or a higher tolerance for mismatches by Dmc1, which may enable it to promote recombination between nonidentical homologs (Steinfeld et al., 2019).

Our analysis of RAD-51 and DMC-1 in *P. pacificus* reveals their distinct contributions during meiosis. The binding of these proteins to chromatin appears very different; the large number of DMC-1 foci suggest that it binds to sites other than repair intermediates. In contrast, RAD-51 displays a more restricted punctate localization, and only after DMC-1 is largely removed from chromosomes upon completion of synapsis. Intriguingly, both DMC-1 and RAD-51 depend on SPO-11 for their association with meiotic chromosomes. We interpret these observations to indicate that DMC-1 is positively regulated by a mechanism that responds to SPO-11 activity, likely through activation of a DNA damage signaling pathway. In contrast, the association of RAD-51

with recombination intermediates may normally be inhibited until after the establishment of CO intermediates between each pair of chromosomes.

The sequential localization of DMC-1 and RAD-51 first suggested that they function independently, and this is further supported by our analysis of loss-of-function mutations. In contrast to budding yeast and *A. thaliana*, we have found that RAD-51 in *P. pacificus* is dispensable for the activity of DMC-1 in pairing, synapsis, and CO formation. Instead, RAD-51 appears to play a supporting role in DSB repair during pachytene, promoting repair of DSBs that remain after CO designation has occurred. In *C. elegans*, which expresses only RAD-51, a similar switch between two modes of DSB repair is nevertheless observed during meiotic prophase: association of RAD-51 with repair intermediates is differentially regulated from the onset of meiosis until a mid-pachytene transition that coincides with CO designation; at this time, cells' competence to convert DSBs to interhomolog COs is also lost (Hayashi et al., 2007). An analogous switch from a "meiotic" repair to a "somatic"-like repair pathway in mid-pachytene is also observed in mouse spermatocytes (Enguita-Marruedo et al., 2019).

Taken together, it appears that DMC-1 and RAD-51 have specialized functions in *P. pacificus*: formation of interhomolog CO intermediates by DMC-1 prior to completion of synapsis, followed by a more generic mode of double-strand break repair by RAD-51. Our observations that nuclei in *rad-51* mutant*s* display cruciform bivalents and lack fragmented chromatin at diakinesis suggests that excess DSBs can be repaired through an alternate pathway that does not depend on RAD-51 activity, such as non-homologous end joining, or that DMC-1 can compensate for loss of RAD-51 but not vice

versa. Future studies may reveal how the activities of RAD-51 and DMC-1 are regulated to accomplish an orderly hand-off during meiotic prophase.

Comparative analysis of meiosis reveals variations and similarities within the nematode lineage

In addition to establishing key aspects of meiosis in *P. pacificus*, this work also illuminates the evolutionary history of meiosis in *C. elegans*. A body of prior work has revealed that recombination-independent homologous synapsis in *C. elegans* relies on Pairing Centers (PCs), specialized chromosome regions that interact with nuclear envelope and drive chromosome movement during early prophase. Similar roles in chromosome movement and pairing during meiosis are typically mediated by telomeres, but have shifted to a unique region on each chromosome in *C. elegans*. PCs in *C. elegans* mediate synapsis-independent pairing and also act as the sites of synapsis initiation (MacQueen 2005, Rog and Dernburg, 2013). In most other organisms, telomere-led chromosome movement is thought to promote homologous interactions, but stabilization of pairing and initiation of synapsis require and often occur at early recombination intermediates, which depend on Spo11 and Dmc1 activity.

PC activity in *C. elegans* depends on and is largely defined by the recruitment of a family of zinc finger proteins that bind to DNA sequence motifs in these regions (Phillips et al., 2009b). These proteins, known as ZIM-1, ZIM-2, and ZIM-3, and HIM-8 in *C. elegans*, act as scaffolds to recruit a cascade of kinase activities required for pairing and synapsis (Harper et al., 2011; Kim et al., 2015; Labella et al., 2011). Pairing Centers have been regarded as an evolutionary alternative to “canonical” Dmc1-

mediated pairing mechanisms, so we found it intriguing that many of the sequenced genomes of nematodes in Clade V include homologs of the HIM-8/ZIM family as well as Dmc1, Hop2, and Mnd1 (Figure 2 – Supplement 1). The *Pristionchus* genus is unusual within this Clade in that it lacks apparent homologs of the PC proteins, while *Caenorhabditis* is among the few genera that lack Dmc1/Mnd1/Hop2, although these genes were independently lost along the branch leading to *Oscheius tipulae*. This suggests that the ability of PCs to trigger homologous synapsis in the absence of DSBs and strand invasion may be recently derived, and perhaps restricted to *Caenorhabditis*.

The existence of PCs in *C. elegans* was initially inferred because chromosome rearrangements often result in asymmetric crossover suppression: regions distal to translocation breakpoints are inhibited from crossing over, while the chromosome region containing the PC undergoes elevated recombination due to a feedback mechanism that helps to ensure an “obligate crossover” (Rose and McKim 1992; Yu et al., 2016). Based on the crossover suppression we observed in constructing a genetic map, it now seems likely that *P. pacificus* may have a PC-like activity localized asymmetrically on its chromosomes. This was unexpected given the absence of obvious homologs of the zinc finger proteins required for PC function in *C. elegans*, and the more “conventional” dependence of pairing and synapsis on recombination that we have documented for *P. pacificus*.

If PCs are indeed conserved in *P. pacificus*, they clearly do not mediate recombination-independent synapsis, as in *C. elegans*. Based on our cytological observations, it is more likely that synapsis initiates at recombination intermediates in *P. pacificus*, although this has not yet been tested rigorously. We speculate that Pairing

Centers may act as a source of a protein factor required for CO designation, and that this factor must move from the source to the site of a recombination intermediate along the SC. According to this model, the SC must eventually span the distance between these two sites for a recombination intermediate to be designated as an eventual CO. For example, in mammals Cdk2 is initially found at telomeres and later at crossover intermediates; perhaps it moves along the SC, thereby ensuring that only recombination intermediates linked in *cis* to homologous telomeres can eventually become crossovers.

Such a mechanism may help to account for the preservation of genetic linkage units known as “Nigon elements” over long evolutionary periods, which has been documented through genome sequencing of diverse nematodes (Foster et al., 2020; Gonzalez de la Rosa et al., 2021; Tandonnet et al., 2019). We have previously speculated that unique PC regions may have arisen in holocentric nematodes as part of a meiotic system that promotes karyotype stability (MacQueen et al., 2005; Rog and Dernburg, 2013), an idea that seems more viable in light of our indirect evidence for their conservation in *Pristionchus*. When inversions arise that suppress local recombination, they can lead to intraspecies reproductive barriers such as toxin/antitoxin systems, and eventually to full speciation.

P. pacificus shares many experimental advantages with *C. elegans* for molecular studies of meiosis. Naturally, it offers a more limited suite of experimental tools, since it was more recently developed and is less widely studied. Genome engineering using CRISPR/Cas9 is less efficient than in *C. elegans*, and has so far been refractory to large insertions, such as transgenes encoding fluorescent proteins. However, this barrier will likely be overcome, just as technical tweaks have greatly improved editing

efficiency in *C. elegans* in less than a decade. Another obstacle is the absence of balancer chromosomes, which are invaluable for maintaining mutations in essential genes in *C. elegans*. Notably, our genetic map data indicating the likely presence of crossover-suppressing rearrangements between divergent strains of *P. pacificus* suggests that it may be possible to propagate balancer chromosomes in this species, which would be valuable additions to the experimental toolbox.

Our work has now established that the recombination landscape is remarkably well conserved between *P. pacificus* and *C. elegans*. This was initially surprising in light of the major differences in their regulation of synapsis and recombination. Indeed, comparison of *P. pacificus* and *C. elegans* reveals that enrichment of COs on the chromosome arms and robust chromosome-wide CO interference can be implemented through divergent meiotic programs, *e.g.*, with synapsis either dependent on or independent of crossover precursors, and with CO sites designated either before or after completion of synapsis. Interestingly, other features of chromosome organization, including enrichment for novel and developmentally-regulated genes on the arms, with more ancestral and broadly expressed genes concentrated in the centers, as well as chromosome-wide chromatin modification profiles, are also conserved across the Rhabditina (Werner et al., 2018). How the recombination landscape is shaped by and/or contributes to these genomic features is not well understood, but the conservation of these features over tens of millions of years of evolution suggests that they are important for genome transmission and/or function.

Nematodes are an ancient and widespread phylum in which most and perhaps all species have holocentric chromosomes. The presence of spindle-attachment sites

along the length of chromosomes poses unique challenges for both mitosis and meiosis (Dernburg, 2001; Melters et al., 2012). In monocentric organisms, the centromeres and/or pericentromeric regions typically recruit factors such as Shugoshin to maintain cohesion between sister chromatids during the first, reductional meiotic division, while release of cohesion along chromosome arms allows segregation of recombinant homologs (Watanabe and Kitajima, 2005). Holocentric chromosomes must use alternate mechanisms to implement the stepwise loss of cohesion needed for two orderly meiotic divisions. The asymmetric SC disassembly we observe in *P. pacificus*, together with our evidence that the orientation of chromosomes during meiotic divisions is stochastically determined by crossover position (Figure 6- Supplemental Figure 2) likely reflects conservation of a mechanism discovered in *C. elegans* in which crossover designation leads to asymmetric SC disassembly, retention of cohesion on one side of the CO site during the first division, and release on the other side (Ferrandiz et al., 2018; Martinez-Perez et al., 2008; Severson and Meyer, 2014; Tzur et al., 2012). Thus, this particular solution to the problem of segregating holocentric chromosomes in meiosis appears to predate the Rhabditine radiation. This pathway relies on the formation of two bivalent “arms” with reciprocal functions, which in turn depends on strict crossover interference; multiple crossovers “confuse” the system and lead to frequent missegregation (Hollis et al., 2020). We expect that these two features of meiosis are widely shared among and perhaps beyond Clade V nematodes. However, they may not be universal among nematodes; for example, studies in Ascarids have shown that heterochromatic regions near one end of a chromosome act as meiotic centromeres and are eliminated in somatic cells (Goday and Pimpinelli, 1989; Melters et

al., 2012). This mechanism may allow for more relaxed CO control and/or a different pattern of COs between homologous chromosomes.

Inexpensive genome sequencing and the adaptability of CRISPR/Cas-based genome editing has enabled rapid progress in developing new experimental models such as *P. pacificus* for molecular studies. Future studies in *P. pacificus* and other nematodes will likely expand our understanding of core mechanisms and plasticity of sexual reproduction.

MATERIALS AND METHODS

P. pacificus *strains and maintenance*

Animals were cultured on NGM media with *E. coli* OP50 at 20°C under the standard conditions developed for *C. elegans* (Brenner, 1974). The wild-type strain in which most mutations were generated was a derivative of PS312 designated as “97.” The Sommer lab found that this isolate was more amenable to genome editing by CRISPR-Cas9 than the parental strain. Mutant alleles were maintained in unbalanced heterozygotes. Every few generations and immediately prior to any analysis, single adult hermaphrodites were picked to new plates and allowed to lay embryos for two days, after which the genotype of the parent was determined by PCR genotyping. Progeny from heterozygous mothers, 25% of which are homozygous for the meiotic mutation, were analyzed using the assays described here; heterozygous and wild-type siblings were frequently used as controls, in addition to unedited wild-type animals.

CRISPR/Cas9-mediated genome editing

To modify the *P. pacificus* genome, we adapted our preferred CRISPR/Cas9 protocol from *C. elegans* to *P. pacificus*. Equimolar quantities of Alt-R®CRISPR-Cas9 crRNA and tracrRNA molecules (Integrated DNA Technologies, Coralville, IA) were hybridized using a thermocycler (95°C for 5 minutes, then 25°C for 5 minutes). 4µl of 100µM hybridized tracrRNA/crRNA was combined with 4µl of 40µM *S. pyogenes* Cas9-NLS purified protein (QB3 MacroLab, UC Berkeley, Berkeley, CA) and incubated at room temperature for 5 minutes. 2µl of 100µM stock of an Ultramer® DNA oligo (IDT)

repair template containing 50-60 bp homology arms and the desired epitope or mutation sequence was added to the mixture, for a total volume of 10µl, and injected into the gonads of young adult hermaphrodites aged 24 hours from the final larval (J4) stage. Following a 2-4 hour recovery period, injected animals were allowed to lay embryos at 20°C for 16-20hr. Four days later, a fraction of the F1 population (typically 150-200 progeny from 6-8 injected P_0s) was screened for the presence of the desired mutation or epitope tag sequence by PCR, and candidate alleles were verified by Sanger sequencing. A complete list of crRNA, repair template, and genotyping primer sequences used to generate alleles in this study is provided as Table S1.

TALEN constructs used in our initial analysis of *dmc-1* and *spo-11* were generated using a protocol adapted from Zhang et al. (2011) and designed using the TAL Effector Nucleotide Targeter 2.0 website (https://tale-nt.cac.cornell.edu/).

Brood analysis

To quantify embryonic viability, brood size, and male progeny of wild-type and *rad-51* mutants, J4 (virgin) hermaphrodites were picked onto individual plates and transferred every 24 hours over 72 hours total. Embryos were counted each day, after transferring the adult hermaphrodite to a new plate, and kept at 20°C. Three to four days later, adults were counted on each plate. To analyze *spo-11* and *dmc-1* mutants, 24 individual J4 hermaphrodites were picked from progeny of a verified heterozygous mutant hermaphrodite. Quantification was performed as in wild type, but after 72 hours, the adult hermaphrodite was lysed and genotyped for the presence of the mutation. Thus, although 24 animals total were quantified from a mixed population of *spo-11/+* or

dmc-1/+ animals, data from 5 homozygous *spo-11* and 7 homozygous *dmc-1* mutant animals are reported in the data table, Figure 5D.

FISH probes

Probes targeting a central locus on Chromosome IV and the left end of Chromosome X were designed based on two short tandem repeat motifs. Tandem Repeat Finder v4.09 (Benson, 1999) was used to identify tandem repeats in *P. pacificus* “El Paco” genome assembly (Rödelsperger et al., 2017) using default parameters and a maximum periodicity of 200 bp. The output was then filtered to identify repeats that spanned more than 8 kb. These were compared to the genome sequence using BLAST to identify the subset of sequences restricted to a single major locus per genome. A subset of these repeats was then tested for specific and robust hybridization with oligonucleotide probes. The Chromosome IV probe (TCATTGAAATGATCACAATCATTGA) targets a 30-base repeated motif ATGATCATTGAAATGATCACAATCATTGAG, which spans 40.1 kb at a position 11.3 Mb from the left end of chromosome IV. The Chromosome X probe (GGTGGTCGACGGCTGCGTCG) targets the 30-base repeat motif GGTGGTCGACGGCTGCGTCGACTGAAGAGT, that spans two very close regions of 29.3 kb and 11.1 kb on the left end of the X chromosome. Single-stranded oligonucleotides labeled at the 3’ end with 6-FAM or Cy3 dyes were purchased from IDT and used directly as FISH probes.

Antibodies

Antibodies against Ppa-RAD-51 were generated against a 6xHis-tagged N-terminal fusion protein (aa 1-103) purified from *E. coli*. Four mice were immunized with the antigen. Serum from one animal, designated S148, was used without purification at 1:300 dilution (Pocono Rabbit Farm and Laboratory, Canadensis, PA). Antibodies against Ppa-HOP-1 were generated by genetic immunization against aa 177-276 (SDIX, Newark, DE) and used in the following experiments at 1:300 dilution. Additional antibodies were purchased from commercial sources and diluted as follows: mouse anti-FLAG (1:500, Sigma #F1804), mouse anti-V5 (1:500, Thermo Fisher #R960-25), rabbit anti-V5 (1:250, Millipore Sigma #V8137), goat anti-HA (1:500, Novus Biologicals #NB600-362), and mouse anti α-tubulin, clone DM1A (1:400, Millipore #05-829). Secondary antibodies raised in donkey and labeled with Alexa 488, Cy3, or Cy5 were used at 1:400 dilution (Jackson ImmunoResearch Laboratories).

Cytological analysis

To stage animals for each experiment, 30-40 J4 larvae were picked from a PCR-verified heterozygous mother onto a fresh plate and allowed to develop for an additional 24 or 48 hours at 20°C. Immunofluorescence and FISH methods for germline tissue were adapted from *C. elegans* (Phillips et al., 2009a), with minor modifications. Briefly, adult hermaphrodites were dissected on a clean coverslip in egg buffer containing 0.05% tetramisole and 0.1% Tween-20. Samples were fixed for 2 minutes in egg buffer containing 1% formaldehyde and then transferred to a 1.5-ml tube containing PBST. After 5 minutes, the buffer was replaced with ice-cold methanol and incubated at room temperature for an additional 5 minutes. Worms were washed twice with PBST, blocked

754 with Roche blocking reagent, and stained with primary antibodies diluted in Roche
755 blocking solution for 1.5-2 hours at room temperature. Samples were washed with
756 PBST and incubated with secondary antibodies raised in donkeys and conjugated with
757 Alexa-488, Cy3 or Cy5 (Jackson ImmunoResearch Laboratories, West Grove, PA).
758 Worms were then incubated with 1μg/ml DAPI in PBST, washed with PBST, and
759 mounted in ProLong™ Gold (Invitrogen) before imaging.

760 For immunofluorescence in embryos, mixed-stage worms were washed off of 20
761 plates in distilled water, pelleted, and treated with household bleach diluted 8-fold with
762 distilled water for 5 minutes at room temperature. Embryos were collected by
763 centrifugation and washed twice with PBS. To dissolve the vitelline membrane, a
764 solution containing 2.6ml of n-heptane, 2ml of PBS, and 1% paraformaldehyde (final)
765 was added to the embryo pellet for 5 minutes at room temperature with shaking.
766 Treated embryos were collected by centrifugation, washed twice with 5ml MeOH, three
767 times with PBS, and incubated with Roche blocking reagent, primary, and secondary
768 antibodies as described above. Embryos were mounted on agarose pads for imaging.

769 To label replicating DNA in proliferating germline stem cells, gonads of age-
770 matched hermaphrodites were injected with 0.3nM Cy3-dUTP solution. After 30 minutes
771 of recovery on seeded plates, worms were dissected and fixed as for
772 immunofluorescence, stained with DAPI, and mounted for imaging.

773 For FISH experiments, age-matched animals were dissected and fixed as for
774 immunofluorescence experiments described above, except that the initial fixation was
775 for 4 minutes in 2% formaldehyde. After incubation in ice-cold methanol, worms were
776 washed with 2x SSCT twice and incubated in 50% 2x SSCT/50% formamide solution

overnight at 37°C. The next day, the worms were transferred to a small PCR tube, excess solution was removed from the sample, and 40µl of hybridization mix containing 250ng of each probe in hybridization buffer (3.5x SSC, 58% formamide, 12.75% dextran sulfate) was added. DNA was denatured by incubation in a thermocycler at 91°C for 2 minutes and incubated overnight at 37°C. Following overnight hybridization, samples were transferred to a 1.5-ml tube and washed twice with 2x SSCT. After 5 minutes, the solution was replaced with fresh 2x SSCT and mounted with ProLong™ Diamond Antifade Mountant with DAPI (Invitrogen).

Images were acquired as stacks of optical sections at 0.2 µm z-spacing using a DeltaVision Elite microscope (GE) with an Olympus 100X NA 1.4 objective. All data were deconvolved using the constrained iterative algorithm included with the softWoRx package (GE) using default cycle numbers and other settings, and maximum-intensity projections were generated for most images presented here. Distances between FISH probes were calculated using 3D peak finding and distance calculation functions within softWoRx. Images were pseudocolored using softWoRx, Fiji (Schindelin et al., 2012)or Adobe Photoshop.

Genetic map construction

We generated a genetic map of *P. pacificus* using a double-cross hybrid strategy that allowed the simultaneous mapping of meiotic crossovers in male spermatocytes and hermaphrodite oocytes (Figure 8A). We began with three parental lines (P0): “CA,” the “wild type” reference strain PS312 from California; “WA,” PS1843 from Washington State; and “LR,” RSB001 from La Réunion Island. These three strains have been

previously used to generate genetic linkage maps (Rödelsperger et al., 2017, Srinivasan et al., 2003, 2002). We crossed these P0 lines to obtain F1 hybrid CA/WA males and CA/LR hermaphrodites. These F1 hybrid types were then mated to produce the F2 generation, so that each F2 inherits a recombinant genome from both of its F1 parents.

F2 progeny were genotyped using a custom sequencing approach: juvenile (unmated) F2 hermaphrodites were placed on individual 60-mm plates and allowed to self-fertilize for 2-3 generations until their bacterial food was depleted. Worms were washed from each plates and genomic DNA was extracted using Qiagen DNeasy Blood & Tissue Kit (Qiagen) and quantified by Qubit (Invitrogen). Because self- and cross-progeny can be temporally intermingled among broods of *P. pacificus*, we genotyped each sample using several SSLP markers (Dieterich et al., 2008) to confirm the presence of the PS1843 (WA) haplotype (Table S3). A total of 93 validated F2 samples were used to construct genomic libraries for whole-genome sequencing using the plexWell LP384 Library Preparation Kit (seqWell), with ~5x shotgun sequence per F2 sample.

To obtain a set of reference variants for use in genotyping, we sequenced the three parental lines: CA and LR at 86x depth and WA at 61x, and mapped to the CA “El Paco” reference genome using bwa-mem2 (v2.0pre2-4-gf06fc0c) (Vasimuddin et al., 2019). Using freebayes (v1.3.1-17-gaa2ace8) (Garrison and Marth, 2012), with the --standard_filters option, we identified 1,395,065 polymorphic sites with that were (1) homozygous for each P0 genotype and within three standard deviations of the mean depth for all three (CA, 47-125, LR, 44-125, WA, 20-111) and (2) biallelic, with a

different nucleotide in one strain relative to the other two. There were 374,862 such cross-informative sites where CA differed from both WA and LR; 490,484 where LR differed from CA and WA; and 529,719 where WA differed from CA and LR. Importantly, these sites were distributed across the genome.

We genotyped each F2 sample for these cross-informative variants in non-overlapping 100 kb blocks spanning the genome. Our crossing scheme gives rise to four possible genotypes at each position (CA/CA, CA/LR, CA/WA, and WA/LR) that can be easily differentiated based on the relative total depth f_{CA}, f_{WA}, and f_{LR} at cross-informative variant sites within a block, where $f_{CA} + f_{WA} + f_{LR} = 1$. Specifically, we called CA/CA if $f_{CA} > 0.95$, CA/LR if $f_{WA}<0.05$ and $|f_{CA}- f_{LR}|>0.1$, etc. (Figure 8 – Supplemental figure 1A). Genotypes not satisfying one of these inequalities were not called. Genomic blocks that contained fewer than 100 diagnostic sites or for which more than 30% of F2 individuals could not be called were not genotyped. Of the 1,567 non-overlapping 100 kb blocks spanning the genome, 1,398 remained after filtering for too few sites, too few individuals genotyped, and segregation distortion ($p\leq0.001$).

By design, our cross generates sex-specific genetic maps, since WA haplotypes can only be transmitted via the sperm of the CA/WA male parent and LR haplotypes can only be transmitted to ova of the CA/LR hermaphrodite parent. Genetic linkage maps were constructed with OneMap (Margarido et al., 2007) using the “F2 backcross“ population type and the “record” algorithm to order markers.

All sequencing data have been submitted to the NIH Sequence Read Archive under accession number PRJNA734516.

Orthology analysis and phylogenetic inference

Accessions to all data used in the orthology analysis and phylogenetic inference are available in Table S2. We downloaded the genomes and annotation files for 66 nematode species (selecting a maximum of two species per genus) from WormBase ParaSite (Howe et al., 2017) and two tardigrade outgroup taxa (*Hysibius dujardini* and *Ramazzottius varieornatus*) from tardigrades.org. We selected the longest isoform of each protein-coding gene in each species using AGAT (version 0.5.1; (Dainat et al., 2020). To infer the nematode phylogeny, we ran BUSCO (version 5.0.0; using the 'metazoa_odb10' dataset (Simão et al., 2015) on all filtered proteomes and used busco2fasta.py (available at https://github.com/lstevens17/busc(Camacho et al., 2009)o2fasta) to extract 534 single-copy orthologs that were present in at least 70% of species. We aligned the orthologous sequences using MAFFT (version 7.475; (Katoh and Standley, 2013)) and inferred gene trees using IQ-TREE (version 2.1.2; (Nguyen et al., 2015)), allowing the substitution model to be automatically selected (Kalyaanamoorthy et al., 2017). We provided the resulting gene trees to ASTRAL-III (version 5.7.4; (Zhang et al., 2018) to infer a species tree. The resulting tree was visualized using iTOL (Letunic and Bork, 2016).

To investigate the presence of meiotic pairing proteins across the nematode phylogeny, we used OrthoFinder (version 2.5.2; (Emms and Kelly, 2015)) to cluster the longest isoforms of each protein-coding gene into orthologous groups (OGs). We identified the *P. pacificus* orthologs of DMC-1, MND-1, HOP-2, and RAD-51 by searching the proteome using BLASTP (version 2.5.0+; with the orthologous protein sequences from *Homo sapiens* as queries and identified the corresponding OGs. We

identified the OG containing the HIM-8/ZIM family using the *C. elegans* transcript IDs. We aligned each OG using MAFFT and inferred a gene tree using IQ-TREE as previously described. Each gene tree was visually inspected using iTOL and presence or absence of a homolog was recorded for each species. For those species that lacked an apparent MND-1 or HOP-2 ortholog, we searched the genome sequence using TBLASTN with the *P. pacificus* orthologs as a query (recording evidence of a homolog as one or more hits with an E-value of < 1e-5). For species which lacked a DMC-1 ortholog, we searched the genome sequence using both the *P. pacificus* DMC-1 and RAD-51 protein sequences as query, and considered hits (E-value < 1e-5) for DMC-1 that were non-overlapping with those for RAD-51 as evidence of a DMC-1 ortholog. For species which lacked a member of the HIM-8/ZIM family, we searched the genome sequence using TBLASTN with the homologous sequence from its closest relative as a query.

Acknowledgements

This work was supported by funding from the Howard Hughes Medical Institute and the Miller Foundation to AFD, as well as a fellowship from the Helen Hay Whitney Foundation to JB. This work used the Vincent J. Coates Genomics Sequencing Laboratory at UC Berkeley, supported by NIH S10 OD018174 Instrumentation Grant. We are grateful to Ralf J. Sommer, Christian Rödelsperger, Ray Hong, and other members of the *P. pacificus* research community for providing strains and abundant helpful advice. We thank members of the Dernburg Lab for helpful discussions about this work and critical reading of the manuscript. We are grateful to the thoughtful

reviewers of the original version of our manuscript, particularly for spurring us to produce a genetic map.

Figure Legends

Figure 1. Germline organization and meiotic nuclear morphology in *P. pacificus* are superficially similar to *C. elegans.* A. Projection image of the distal arm of a *P. pacificus* hermaphrodite gonad stained with DAPI. Scale bar, 30 µm. Insets show representative nuclei from the premeiotic region (PM), transition zone (TZ), pachytene (Pach), diplotene (Dip), diffuse stage (Diff) and diakinesis. Scale bar, 5 µm. B. Distal region of a *P. pacificus* germline following injection of fluorescent nucleotides to label replicating DNA. Scale bar, 30 µm. C. Metaphase I oocyte expressing CENP-C::V5, stained with anti-V5, DAPI, and anti-tubulin. Scale bar, 10 µm. D. Mitotic chromosomes (DAPI) in the premeiotic germline of adult hermaphrodites and a 2-4 cell stage embryo and expressing CENP-C::V5 (magenta). Scale bar, 2 µm.

Figure 2. Stable homolog pairing requires DSBs and strand invasion. A. Diagram showing the locations of tandem repeat sequences used to generate DNA FISH probes for pairing analysis in *P. pacificus*. B. Representative images show the progression of homolog pairing of Chromosome X (magenta) and Chromosome IV (yellow) during meiotic prophase in wild-type hermaphrodites. Premeiotic region (PM), transition zone (TZ), and pachytene (Pach). Scale bar, 5 µm. C. Representative images of FISH probe signals in *spo-11*, *dmc-1*, and *rad-51* mutants during mid-prophase stage (roughly equivalent to the pachytene stage in wild-type germlines). Scale bar, 5 µm. D. Temporal

progression of X and IV chromosome pairing in WT, *spo-11, dmc-1*, and *rad-51* mutants. Graphs show the distribution of distances within each of 5 equally-sized zones spanning meiotic prophase. E. Distance between pairs of heterologous FISH signals were measured in premeiotic (PM) and transition zone (TZ) nuclei in WT, *spo-11* and *dmc-1* mutants (spanning zones 1 and 2 only). Distances between pairs of homologous FISH signals (Chr. X and IV combined) in TZ nuclei are included for comparison. ***p<.0001, by Student's *t*-test.

Figure 2- figure supplement 1. Presence of meiotic pairing proteins across the nematode phylogeny. D= Dmc1; M=Mnd1; H=Hop2; Z=HIM-8/ZIM-1,2,3. Circles indicate the presence of a homolog; solid outlines indicate homologs identified via orthology clustering; dashed outlines represent evidence of a homolog from TBLASTN searches of the genome sequence. *C. elegans* and *P. pacificus* are highlighted in blue. Major nematode clades are highlighted. Phylogeny rooted on two tardigrade species (*Hysibius exemplaris* and *Ramazzottius varieornatus*); not shown. Branch lengths are not shown.

Figure 2- figure supplement 2. A. Composite projection images of whole gonads stained with DAPI from WT, *spo-11*, *dmc-1*, and *rad-51* mutants. The extent of the transition zone of each gonad is indicated with dashed lines. Scale bar, 30 µm. B. Quantification of transition zone length as a fraction of the distance from meiotic onset to the end of pachytene in WT (n=7), *spo-11* (n=7), *dmc-1* (n=7), and *rad-51* (n=10).

Error bars indicate mean ± SD. *spo-11* and *dmc-1* mutants show significant differences from WT ($p<0.0001$) but not *Ppa-rad-51* ($p=0.8426$) by ordinary one-way ANOVA.

Figure 3. SPO-11 and DMC-1 are required for homologous synapsis in *P. pacificus*, while RAD-51 is dispensable. A. Composite projection image of a wild-type strain expressing SYP-4::HA, stained with DAPI (gray), anti-HOP-1 (red), and anti-HA (green). Meiosis progresses from left to right. Scale bar, 30 µm. B. Higher magnification images of wild-type nuclei in the premeiotic region (PM), transition zone (TZ), pachytene (Pach), and diplotene (D) stages. C. Localization of SYP-4::HA and HOP-1 in WT, *spo-11*, *dmc-1*, and *rad-51* mutants during early and mid-prophase (roughly equivalent to the TZ and pachytene regions in wild-type germlines, respectively). Synapsis fails in the absence of *spo-11* and *dmc-1* function but occurs normally in *rad-51* mutants. Scale bar, 5 µm.

Figure 3- figure supplement 1. All epitope-tagged proteins described in this study support normal meiosis. Epitope-tagged alleles were generated by in-frame insertion into the endogenous gene loci using CRISPR/Cas9 (see Materials and Methods), and homozygosed by selfing of successfully edited progeny. Fidelity of meiotic segregation in the resulting strains was analyzed by counting the frequency of viable embryos and male progeny among whole broods from self-fertilizing hermaphrodites, as indicated. Quantification of wild-type broods is also reported in Figure 5D.

Figure 4. DMC-1 and RAD-51 localize sequentially to meiotic chromosomes. A. Composite projection image of a wild-type gonad expressing DMC-1::V5, stained with

DAPI (blue), anti-V5 (magenta), and anti-RAD-51 (yellow). Meiotic progression is from left to right. Scale bar, 30 μm. Inset shows the distinct localization of DMC-1 (magenta) and RAD-51 (yellow) in the transition zone and pachytene regions, respectively. Scale bar, 5 μm. B. Higher magnification images of nuclei in the transition zone and pachytene region. DMC-1 is present along chromatin in the transition zone and disappears at pachytene. By contrast, RAD-51 localizes to discrete foci starting at pachytene. Scale bar, 5 μm. C. Occasional nuclei at the transition from leptotene-zyogtene to pachytene are positive for both DMC-1 and RAD-51. The signals do not completely overlap. Scale bar, 2 μm. D. Example of a nucleus with polarized DAPI morphology and strong DMC-1 signal during later prophase. Such “straggler” cells may be delayed in completing synapsis or undergoing apoptosis. Scale bar, 2 μm.

Figure 4- figure supplement 1. A. Localization of RAD-51::V5. Composite projection image of a wild-type gonad expressing RAD-51::V5, stained with DAPI and anti-V5. Meiotic progression is from left to right. Scale bar, 30 μm. DMC-1 and RAD-51 localize to meiotic chromosomes independently of each other, but both require SPO-11. B. DMC-1 (magenta) is abundant on chromosomes in transition zone nuclei of *rad-51* mutants. Anti-RAD-51 immunofluorescence was used to identify homozygous mutants among the progeny of heterozygotes. C. RAD-51 foci are observed in late pachytene nuclei of *dmc-1* mutants, proximal to the extended transition zone. RAD-51 foci appear larger and more numerous than in wild-type pachytene nuclei. D. DMC-1 forms nuclear aggregates in *spo-11* mutants and does not localize along chromosomes. E and F.

RAD-51 foci are detected in premeiotic nuclei of *spo-11* mutants but are absent during meiotic prophase. Scale bar, 5 µm.

Figure 5. CO formation requires SPO-11 and DMC-1, but not RAD-51. A. Representative images of DAPI-staining bodies at diakinesis for each indicated genotype. Scale bar, 5 µm. B. Quantification of DAPI-staining bodies in the "-1" oocyte (immediately distal to the spermatheca) at diakinesis for each indicated genotype (*n*= represents number of nuclei scored). C. Quantification of gonads which lacked nuclei with DAPI-staining bodies at diakinesis stage. *n* is the number of germlines scored for each genotype. D. Frequencies of viable embryos and male progeny of whole broods from wild type, *spo-11*, *dmc-1* and *rad-51* mutant hermaphrodites.

Figure 6. COSA-1 accumulates at a single focus per chromosome pair. A. Composite projection image of a wild-type strain expressing three epitope-tagged proteins (COSA-1::3xFLAG, DMC-1::V5, and SYP-4::HA), stained with anti-FLAG, anti-V5 and anti-HA antibodies. Scale bar, 30 µm. B. Higher magnification images of nuclei from the transition zone (TZ), pachytene (pach), mid- and late diplotene (D). COSA-1::3xFLAG (green) foci are detected in transition zone nuclei but do not colocalize with DMC-1::V5 (cyan). Foci peak in brightness in pachytene nuclei and gradually become dimmer until they are no longer detected during late diplotene. In early to mid-diplotene nuclei, six short stretches of SYP-4::HA (magenta) are observed per nucleus, each associated with a single COSA-1::3xFLAG focus. Scale bar, 5 µm. C. Histogram showing the number of COSA-1::3xFLAG foci observed per nucleus in the pachytene region.

Analysis was restricted to 15 nuclei per gonad immediately proximal to the transition zone and lacking DMC-1::V5 signal. Five individual gonads were analyzed, for a total of 75 nuclei scored. D. Partial projection of a representative nucleus in mid to late diplotene, stained with anti-HOP-1 (blue), anti-HA (marking the SC, magenta), and anti-FLAG (marking COSA-1, green). A single COSA-1::3xFLAG focus is observed at a junction (marked with a red arrowhead) between the “short arm,” where SYP-4::HA is retained, and splayed “long arms” lacking SC but positive for HOP-1. Scale bar, 2 µm.

Figure 6 - figure supplement 1. COSA-1 accumulates at a single site per chromosome pair during spermatogenesis. A. Composite projection image of a wild-type gonad from a J4-stage hermaphrodite expressing COSA-1::3xFLAG (green) and SYP-4::HA (magenta). Scale bar, 30 µm. At this stage the germline is still undergoing spermatogenesis. Inset shows a higher magnification image of nuclei in the pachytene region. As during oogenesis, ~6 COSA-1::3xFLAG foci are observed in pachytene nuclei during spermatogenesis. Scale bar, 5 µm.

Figure 6 - Supplemental Video 1. COSA-1/Cntd1 accumulates at a single site per chromosome pair. 3D volume rendering of a single nucleus from the pachytene region of a wild-type worm expressing COSA-1::3xFLAG (green) and SYP-4::HA (magenta). Each frame is a maximum intensity projection from a region of a deconvolved 3D image. Each stretch of SYP-4::HA is associated with a COSA-1::3xFLAG focus.

Figure 6 - figure supplement 2. Asymmetric disassembly of the synaptonemal complex can occur along either arm of bivalent chromosomes. Projection images of representative wild-type diplotene nuclei expressing SYP-4::HA, hybridized with a fluorescent probe specific for the left end of chromosome X (magenta), and stained with anti-HA (yellow) and DAPI (blue). A. Nuclei in which the FISH signal recognizes the "long arm" lacking SYP-4::HA. B. Nuclei in which the probe recognizes the "short arm" that retains SYP-4::HA. Scale bar, 2 μm.

Figure 7. COSA-1::3xFLAG accumulates at sites of presumptive COs. A. Nuclei from hermaphrodites of the indicated genotype displaying COSA-1::3xFLAG (green) in early and mid-prophase (roughly equivalent to the transition zone and pachytene regions in wild-type germlines, respectively). COSA-1 foci are absent in *dmc-1* mutants, but 6 foci per nucleus are detected in wild type and *rad-51* mutants. Occasional foci are detected in s*po-11* mutants. Scale bar, 5 μm.

Figure 8. A. Crossing scheme to generate a recombination map using three parental strains. California PS312 (CA), Washington PS1843 (WA), and La Réunion Island RSB001 (LR) strains were crossed to obtain F1 hybrids, which were then crossed to each other. Whole genome sequencing of progeny from crosses between hybrid F1s enabled the analysis of meiotic recombination events in each F1 parent. B. Genotype transitions along a chromosome in F2 correspond to recombination in the male or hermaphrodite F1 parent. C. Marey plots show genetic map position in centimorgans vs. the physical position in megabases for male (green) and hermaphrodite (magenta)

meiosis. Each bin was treated as a single locus and dots were plotted at the center of each marker bin. Map positions were computed with OneMap as described. The observed map length of ~50 cM indicates that chromosomes undergo an average of 1 CO per meiosis. The X chromosome lacks a homolog in males, so there is no male-specific map for the X in our data.

Figure 8 – figure supplement 1. A. Genotyping. For each 100 kb genomic block, progeny were genotyped based on the number of CA-, WA-, and LR-specific variants they contained, given the expectation of four possible genotypes CA/CA, CA/LR, WA/CA, WA/LR. In scatterplot each point represents s a single bin in a specific individual, with $X = f_{WA} + f_{LR} - 2f_{CA}$, and $Y = f_{LR} - f_{WA}$. Gray dots represent genotypes that are conservatively left as “not called.” B. Genotypes of the mapping panel. F2 genotypes inherited from male (left) and hermaphrodite (right) parents. Each thin row is one progeny. White vertical stripes represent 100 kb windows that could not be reliably genotyped due to low numbers of P0-specific variant sites and/or sequencing depth of progeny.

Table S1. Genes, alleles, and genome editing reagents used in this manuscript.

Table S2. Species names and sequence accession numbers used for the phylogenetic analysis summarized in Figure 2 – Figure Supplement 1.

Table S3. SSLP markers and genotyping primers used to confirm cross-progeny for genetic map construction.

Table S4. Software version numbers and parameters used in this work.

Table S5. Genotype calls for the 93 individual F2 progeny used for mapping crossovers in hermaphrodite oocytes. Each column represents one hybrid progeny in arbitrary order. "A" genotypes are inherited from the California PS312 (CA), F0 parent, "R" genotyes are inherited from the La Réunion Island RSB001 F0 parent

Table S6. Genotype calls for the 93 individual F2 progeny used for mapping crossovers in male spermatocytes. Each column represents one hybrid progeny in arbitrary order (same order as in Table S5). The "A" genotypes were inherited from the California PS312 (CA), F0 parent, "W" genotypes are inherited from the Washington PS1843 F0 parent.

Table S7. Map distances in centimorgans (cM) generated with OneMap based on the data in Tables S5 and S6, using the 'record' algorithm.

Table S8. Summary of crossovers detected on each chromosome in oocytes (XX) and spermatocytes (XO), including the number of nonrecombinant chromatids and chromatids with 1 or 2 crossovers. No higher-order recombinant chromatids were observed.

Literature and software cited

Albertson DG, Thomson JN. 1993. Segregation of holocentric chromosomes at meiosis in the nematode,Caenorhabditis elegans. *Chromosome Res* **1**:15–26. doi:10.1007/BF00710603

Aravind L, Koonin EV. 1998. The HORMA domain: a common structural denominator in mitotic checkpoints, chromosome synapsis and DNA repair. *Trends in Biochemical Sciences* **23**:284–286. doi:10.1016/S0968-0004(98)01257-2

Barnes TM, Kohara Y, Coulson A, Hekimi S. 1995. Meiotic recombination, noncoding DNA and genomic organization in Caenorhabditis elegans. *Genetics* **141**:159.

Bergerat A, de Massy B, Gadelle D, Varoutas P-C, Nicolas A, Forterre P. 1997. An atypical topoisomerase II from archaea with implications for meiotic recombination. *Nature* **386**:414–417. doi:10.1038/386414a0

Bishop DK, Park D, Xu L, Kleckner N. 1992. DMC1: A meiosis-specific yeast homolog of E. coli recA required for recombination, synaptonemal complex formation, and cell cycle progression. *Cell* **69**:439–456. doi:10.1016/0092-8674(92)90446-J

Brenner S. 1974. The genetics of Caenorhabditis elegans. *Genetics* **77**:71–94.

Camacho C, Coulouris G, Avagyan V, Ma N, Papadopoulos J, Bealer K, Madden TL. 2009. BLAST+: architecture and applications. *BMC Bioinformatics* **10**:421. doi:10.1186/1471-2105-10-421

Christophorou N, Rubin T, Bonnet I, Piolot T, Arnaud M, Huynh J-R. 2015. Microtubule-driven nuclear rotations promote meiotic chromosome dynamics. *Nat Cell Biol* **17**:1388–1400. doi:10.1038/ncb3249

Christophorou N, Rubin T, Huynh J-R. 2013. Synaptonemal Complex Components Promote Centromere Pairing in Pre-meiotic Germ Cells. *PLoS Genet* **9**:e1004012. doi:10.1371/journal.pgen.1004012

Cloud V, Chan Y-L, Grubb J, Budke B, Bishop DK. 2012. Rad51 Is an Accessory Factor for Dmc1-Mediated Joint Molecule Formation During Meiosis. *Science* **337**:1222–1225. doi:10.1126/science.1219379

Couteau F, Belzile F, Horlow C, Grandjean O, Vezon D, Doutriaux M-P. 1999. Random Chromosome Segregation without Meiotic Arrest in Both Male and Female Meiocytes of a dmc1 Mutant of Arabidopsis. *The Plant Cell* **11**:1623. doi:10.2307/3871042

Da Ines O, Degroote F, Goubely C, Amiard S, Gallego ME, White CI. 2013. Meiotic Recombination in Arabidopsis Is Catalysed by DMC1, with RAD51 Playing a Supporting Role. *PLoS Genet* **9**:e1003787. doi:10.1371/journal.pgen.1003787

Dainat J, Hereñú D, Pucholt P. 2020. NBISweden/AGAT: AGAT-v0.5.1. Zenodo. doi:10.5281/ZENODO.4205393

Dernburg AF. 2001. Here, there, and everywhere: kinetochore function on holocentric chromosomes. *J Cell Biol* **153**:F33-38. doi:10.1083/jcb.153.6.f33

Dieterich C, Clifton SW, Schuster LN, Chinwalla A, Delehaunty K, Dinkelacker I, Fulton L, Fulton R, Godfrey J, Minx P, Mitreva M, Roeseler W, Tian H, Witte H, Yang S-P, Wilson RK, Sommer RJ. 2008. The Pristionchus pacificus genome provides a unique perspective on nematode lifestyle and parasitism. *Nat Genet* **40**:1193–1198. doi:10.1038/ng.227

Doyle SR, Laing R, Bartley DJ, Britton C, Chaudhry U, Gilleard JS, Holroyd N, Mable BK, Maitland K, Morrison AA, Tait A, Tracey A, Berriman M, Devaney E, Cotton JA, Sargison ND. 2018. A Genome Resequencing-Based Genetic Map Reveals the Recombination Landscape of an Outbred Parasitic Nematode in the Presence of Polyploidy and Polyandry. *Genome Biology and Evolution* **10**:396–409. doi:10.1093/gbe/evx269

Emms DM, Kelly S. 2015. OrthoFinder: solving fundamental biases in whole genome comparisons dramatically improves orthogroup inference accuracy. *Genome Biol* **16**:157. doi:10.1186/s13059-015-0721-2

Enguita-Marruedo A, Martín-Ruiz M, García E, Gil-Fernández A, Parra MT, Viera A, Rufas JS, Page J. 2019. Transition from a meiotic to a somatic-like DNA damage response during the pachytene stage in mouse meiosis. *PLoS Genet* **15**:e1007439. doi:10.1371/journal.pgen.1007439

Ferrandiz N, Barroso C, Telecan O, Shao N, Kim H-M, Testori S, Faull P, Cutillas P, Snijders AP, Colaiácovo MP, Martinez-Perez E. 2018. Spatiotemporal regulation of Aurora B recruitment ensures release of cohesion during C. elegans oocyte meiosis. *Nat Commun* **9**:834. doi:10.1038/s41467-018-03229-5

Foster JM, Grote A, Mattick J, Tracey A, Tsai Y-C, Chung M, Cotton JA, Clark TA, Geber A, Holroyd N, Korlach J, Li Y, Libro S, Lustigman S, Michalski ML, Paulini M, Rogers MB, Teigen L, Twaddle A, Welch L, Berriman M, Dunning Hotopp JC, Ghedin E. 2020. Sex chromosome evolution in parasitic nematodes of humans. *Nat Commun* **11**:1964. doi:10.1038/s41467-020-15654-6

Garrison E, Marth G. 2012. Haplotype-based variant detection from short-read sequencing. *arXiv:12073907 [q-bio]*.

Goday C, Pimpinelli S. 1989. Centromere organization in meiotic chromosomes of Parascaris univalens. *Chromosoma* **98**:160–166. doi:10.1007/BF00329679

Gonzalez de la Rosa PM, Thomson M, Trivedi U, Tracey A, Tandonnet S, Blaxter M. 2021a. A telomere-to-telomere assembly of *Oscheius tipulae* and the evolution of rhabditid nematode chromosomes. *G3 Genes|Genomes|Genetics* **11**:1–17. doi:10.1093/g3journal/jkaa020

Gonzalez de la Rosa PM, Thomson M, Trivedi U, Tracey A, Tandonnet S, Blaxter M. 2021b. A telomere-to-telomere assembly of *Oscheius tipulae* and the evolution of rhabditid nematode chromosomes. *G3 Genes|Genomes|Genetics* **11**:1–17. doi:10.1093/g3journal/jkaa020

Goodenough U, Heitman J. 2014. Origins of Eukaryotic Sexual Reproduction. *Cold Spring Harbor Perspectives in Biology* **6**:a016154–a016154. doi:10.1101/cshperspect.a016154

Grelon M. 2001. AtSPO11-1 is necessary for efficient meiotic recombination in plants. *The EMBO Journal* **20**:589–600. doi:10.1093/emboj/20.3.589

Harper NC, Rillo R, Jover-Gil S, Assaf ZJ, Bhalla N, Dernburg AF. 2011. Pairing Centers Recruit a Polo-like Kinase to Orchestrate Meiotic Chromosome Dynamics in C. elegans. *Developmental Cell* **21**:934–947. doi:10.1016/j.devcel.2011.09.001

Hayashi M, Chin GM, Villeneuve AM. 2007. C. elegans Germ Cells Switch between Distinct Modes of Double-Strand Break Repair During Meiotic Prophase Progression. *PLoS Genet* **3**:e191. doi:10.1371/journal.pgen.0030191

Hollingsworth NM, Byers B. 1989. HOP1: a yeast meiotic pairing gene. *Genetics* **121**:445–462.

Hollis JA, Glover ML, Schlientz AJ, Cahoon CK, Bowerman B, Wignall SM, Libuda DE. 2020. Excess crossovers impede faithful meiotic chromosome segregation in C. elegans. *PLoS Genet* **16**:e1009001. doi:10.1371/journal.pgen.1009001

Hong RL, Sommer RJ. 2006. Pristionchus pacificus: a well-rounded nematode. *Bioessays* **28**:651–659. doi:10.1002/bies.20404

Howe KL, Bolt BJ, Shafie M, Kersey P, Berriman M. 2017. WormBase ParaSite − a comprehensive resource for helminth genomics. *Molecular and Biochemical Parasitology* **215**:2–10. doi:10.1016/j.molbiopara.2016.11.005

Hunter N. 2015. Meiotic Recombination: The Essence of Heredity. *Cold Spring Harb Perspect Biol* a016618. doi:10.1101/cshperspect.a016618

Kalyaanamoorthy S, Minh BQ, Wong TKF, von Haeseler A, Jermiin LS. 2017. ModelFinder: fast model selection for accurate phylogenetic estimates. *Nat Methods* **14**:587–589. doi:10.1038/nmeth.4285

Katoh K, Standley DM. 2013. MAFFT Multiple Sequence Alignment Software Version 7: Improvements in Performance and Usability. *Molecular Biology and Evolution* **30**:772–780. doi:10.1093/molbev/mst010

Keeney S, Giroux CN, Kleckner N. 1997. Meiosis-Specific DNA Double-Strand Breaks Are Catalyzed by Spo11, a Member of a Widely Conserved Protein Family. *Cell* **88**:375–384. doi:10.1016/S0092-8674(00)81876-0

Kim Y, Kostow N, Dernburg AF. 2015. The Chromosome Axis Mediates Feedback Control of CHK-2 to Ensure Crossover Formation in C. elegans. *Developmental Cell* **35**:247–261. doi:10.1016/j.devcel.2015.09.021

Kohl KP, Sekelsky J. 2013. Meiotic and Mitotic Recombination in Meiosis. *Genetics* **194**:327–334. doi:10.1534/genetics.113.150581

Labella S, Woglar A, Jantsch V, Zetka M. 2011. Polo Kinases Establish Links between Meiotic Chromosomes and Cytoskeletal Forces Essential for Homolog Pairing. *Developmental Cell* **21**:948–958. doi:10.1016/j.devcel.2011.07.011

Lake CM, Hawley RS. 2012. The Molecular Control of Meiotic Chromosomal Behavior: Events in Early Meiotic Prophase in *Drosophila* Oocytes. *Annu Rev Physiol* **74**:425–451. doi:10.1146/annurev-physiol-020911-153342

Letunic I, Bork P. 2016. Interactive tree of life (iTOL) v3: an online tool for the display and annotation of phylogenetic and other trees. *Nucleic Acids Res* **44**:W242–W245. doi:10.1093/nar/gkw290

Lo T-W, Pickle CS, Lin S, Ralston EJ, Gurling M, Schartner CM, Bian Q, Doudna JA, Meyer BJ. 2013. Precise and Heritable Genome Editing in Evolutionarily Diverse Nematodes Using TALENs and CRISPR/Cas9 to Engineer Insertions and Deletions. *Genetics* **195**:331–348. doi:10.1534/genetics.113.155382

MacQueen AJ. 2002. Synapsis-dependent and -independent mechanisms stabilize homolog pairing during meiotic prophase in C. elegans. *Genes & Development* **16**:2428–2442. doi:10.1101/gad.1011602

MacQueen AJ, Phillips CM, Bhalla N, Weiser P, Villeneuve AM, Dernburg AF. 2005. Chromosome Sites Play Dual Roles to Establish Homologous Synapsis during Meiosis in C. elegans. *Cell* **123**:1037–1050. doi:10.1016/j.cell.2005.09.034

Margarido GRA, Souza AP, Garcia AAF. 2007. OneMap: software for genetic mapping in outcrossing species: OneMap. *Hereditas* **144**:78–79. doi:10.1111/j.2007.0018-0661.02000.x

Martinez-Perez E, Schvarzstein M, Barroso C, Lightfoot J, Dernburg AF, Villeneuve AM. 2008. Crossovers trigger a remodeling of meiotic chromosome axis composition that is linked to two-step loss of sister chromatid cohesion. *Genes & Development* **22**:2886–2901. doi:10.1101/gad.1694108

Melters DP, Paliulis LV, Korf IF, Chan SWL. 2012. Holocentric chromosomes: convergent evolution, meiotic adaptations, and genomic analysis. *Chromosome Res* **20**:579–593. doi:10.1007/s10577-012-9292-1

Nadarajan S, Lambert TJ, Altendorfer E, Gao J, Blower MD, Waters JC, Colaiácovo MP. 2017. Polo-like kinase-dependent phosphorylation of the synaptonemal complex protein SYP-4 regulates double-strand break formation through a negative feedback loop. *eLife* **6**:e23437. doi:10.7554/eLife.23437

Namai S, Sugimoto A. 2018. Transgenesis by microparticle bombardment for live imaging of fluorescent proteins in Pristionchus pacificus germline and early embryos. *Dev Genes Evol* **228**:75–82. doi:10.1007/s00427-018-0605-z

Nguyen L-T, Schmidt HA, von Haeseler A, Minh BQ. 2015. IQ-TREE: A Fast and Effective Stochastic Algorithm for Estimating Maximum-Likelihood Phylogenies. *Molecular Biology and Evolution* **32**:268–274. doi:10.1093/molbev/msu300

Pattabiraman D, Roelens B, Woglar A, Villeneuve AM. 2017. Meiotic recombination modulates the structure and dynamics of the synaptonemal complex during *C. elegans* meiosis (preprint). Genetics. doi:10.1101/110064

Penkner A, Tang L, Novatchkova M, Ladurner M, Fridkin A, Gruenbaum Y, Schweizer D, Loidl J, Jantsch V. 2007. The Nuclear Envelope Protein Matefin/SUN-1 Is Required for Homologous Pairing in C. elegans Meiosis. *Developmental Cell* **12**:873–885. doi:10.1016/j.devcel.2007.05.004

Penkner AM, Fridkin A, Gloggnitzer J, Baudrimont A, Machacek T, Woglar A, Csaszar E, Pasierbek P, Ammerer G, Gruenbaum Y, Jantsch V. 2009. Meiotic Chromosome Homology Search Involves Modifications of the Nuclear Envelope Protein Matefin/SUN-1. *Cell* **139**:920–933. doi:10.1016/j.cell.2009.10.045

Phillips CM, Dernburg AF. 2006. A Family of Zinc-Finger Proteins Is Required for Chromosome-Specific Pairing and Synapsis during Meiosis in C. elegans. *Developmental Cell* **11**:817–829. doi:10.1016/j.devcel.2006.09.020

Phillips CM, McDonald KL, Dernburg AF. 2009a. Cytological Analysis of Meiosis in Caenorhabditis elegans In: Keeney S, editor. Meiosis, Methods in Molecular Biology. Totowa, NJ: Humana Press. pp. 171–195. doi:10.1007/978-1-60761-103-5_11

Phillips CM, Meng X, Zhang L, Chretien JH, Urnov FD, Dernburg AF. 2009b. Identification of chromosome sequence motifs that mediate meiotic pairing and synapsis in C. elegans. *Nat Cell Biol* **11**:934–942. doi:10.1038/ncb1904

Phillips CM, Wong C, Bhalla N, Carlton PM, Weiser P, Meneely PM, Dernburg AF. 2005. HIM-8 Binds to the X Chromosome Pairing Center and Mediates Chromosome-Specific Meiotic Synapsis. *Cell* **123**:1051–1063. doi:10.1016/j.cell.2005.09.035

Pittman DL, Cobb J, Schimenti KJ, Wilson LA, Cooper DM, Brignull E, Handel MA, Schimenti JC. 1998. Meiotic Prophase Arrest with Failure of Chromosome Synapsis in Mice Deficient for Dmc1 , a Germline-Specific RecA Homolog. *Molecular Cell* **1**:697–705. doi:10.1016/S1097-2765(00)80069-6

Rockman MV, Kruglyak L. 2009. Recombinational Landscape and Population Genomics of Caenorhabditis elegans. *PLoS Genet* **5**:e1000419. doi:10.1371/journal.pgen.1000419

Rockmill B, Sym M, Scherthan H, Roeder GS. 1995. Roles for two RecA homologs in promoting meiotic chromosome synapsis. *Genes & Development* **9**:2684–2695. doi:10.1101/gad.9.21.2684

Rödelsperger C, Meyer JM, Prabh N, Lanz C, Bemm F, Sommer RJ. 2017. Single-Molecule Sequencing Reveals the Chromosome-Scale Genomic Architecture of the Nematode Model Organism Pristionchus pacificus. *Cell Reports* **21**:834–844. doi:10.1016/j.celrep.2017.09.077

Rog O, Dernburg AF. 2013. Chromosome pairing and synapsis during Caenorhabditis elegans meiosis. *Current Opinion in Cell Biology* **25**:349–356. doi:10.1016/j.ceb.2013.03.003

Rose AM, McKIM KS. 1992. Meiotic Recombination in Caenorhabditis elegansMechanisms of Eukaryotic DNA Recombination. Elsevier. pp. 113–124. doi:10.1016/B978-0-12-293445-2.50014-4

Rudel D, Riebesell M, Sommer RJ. 2005. Gonadogenesis in Pristionchus pacificus and organ evolution: development, adult morphology and cell–cell interactions in the hermaphrodite gonad. *Developmental Biology* **277**:200–221. doi:10.1016/j.ydbio.2004.09.021

Sato A, Isaac B, Phillips CM, Rillo R, Carlton PM, Wynne DJ, Kasad RA, Dernburg AF. 2009. Cytoskeletal Forces Span the Nuclear Envelope to Coordinate Meiotic Chromosome Pairing and Synapsis. *Cell* **139**:907–919. doi:10.1016/j.cell.2009.10.039

Schindelin J, Arganda-Carreras I, Frise E, Kaynig V, Longair M, Pietzsch T, Preibisch S, Rueden C, Saalfeld S, Schmid B, Tinevez J-Y, White DJ, Hartenstein V, Eliceiri K, Tomancak P, Cardona A. 2012. Fiji: an open-source platform for biological-image analysis. *Nat Methods* **9**:676–682. doi:10.1038/nmeth.2019

Severson AF, Meyer BJ. 2014. Divergent kleisin subunits of cohesin specify mechanisms to tether and release meiotic chromosomes. *eLife* **3**:e03467. doi:10.7554/eLife.03467

Shakes DC, Wu J, Sadler PL, LaPrade K, Moore LL, Noritake A, Chu DS. 2009. Spermatogenesis-Specific Features of the Meiotic Program in Caenorhabditis elegans. *PLoS Genet* **5**:e1000611. doi:10.1371/journal.pgen.1000611

Simão FA, Waterhouse RM, Ioannidis P, Kriventseva EV, Zdobnov EM. 2015. BUSCO: assessing genome assembly and annotation completeness with single-copy orthologs. *Bioinformatics* **31**:3210–3212. doi:10.1093/bioinformatics/btv351

Sommer RJ, editor. 2015. Pristionchus pacificus: a nematode model for comparative and evolutionary biology, Nematology monographs and perspectives. Leiden□; Boston: Brill.

Sommer RJ, Carta LK, Kim S-Y, Sternberg PW. 1996. Morphological, genetic and molecular description of Pristionchus pacificus sp. N. (Nematoda: Neodiplogastridae). *Fundam appl Nematol* **19**:511–521.

Srinivasan J, Sinz W, Jesse T, Wiggers-Perebolte L, Jansen K, Buntjer J, van der Meulen M, Sommer RJ. 2003. An integrated physical and genetic map of the nematode Pristionchus pacificus. *Mol Gen Genomics* **269**:715–722. doi:10.1007/s00438-003-0881-8

Srinivasan J, Sinz W, Lanz C, Brand A, Nandakumar R, Raddatz G, Witte H, Keller H, Kipping I, Pires-daSilva A, Jesse T, Millare J, de Both M, Schuster SC, Sommer RJ. 2002. A bacterial artificial chromosome-based genetic linkage map of the nematode Pristionchus pacificus. *Genetics* **162**:129–134.

Steinfeld JB, Beláň O, Kwon Y, Terakawa T, Al-Zain A, Smith MJ, Crickard JB, Qi Z, Zhao W, Rothstein R, Symington LS, Sung P, Boulton SJ, Greene EC. 2019. Defining the influence of Rad51 and Dmc1 lineage-specific amino acids on genetic recombination. *Genes Dev* **33**:1191–1207. doi:10.1101/gad.328062.119

Tandonnet S, Koutsovoulos GD, Adams S, Cloarec D, Parihar M, Blaxter ML, Pires-daSilva A. 2019. Chromosome-Wide Evolution and Sex Determination in the Three-Sexed Nematode <i/> *Auanema rhodensis*. *G3* g3.0011.2019. doi:10.1534/g3.119.0011

Tzur YB, Egydio de Carvalho C, Nadarajan S, Van Bostelen I, Gu Y, Chu DS, Cheeseman IM, Colaiácovo MP. 2012. LAB-1 Targets PP1 and Restricts Aurora B Kinase upon Entrance into Meiosis to Promote Sister Chromatid Cohesion. *PLoS Biol* **10**:e1001378. doi:10.1371/journal.pbio.1001378

Vader G, Musacchio A. 2014. HORMA Domains at the Heart of Meiotic Chromosome Dynamics. *Developmental Cell* **31**:389–391. doi:10.1016/j.devcel.2014.11.009

Vasimuddin Md, Misra S, Li H, Aluru S. 2019. Efficient Architecture-Aware Acceleration of BWA-MEM for Multicore Systems2019 IEEE International Parallel and Distributed Processing Symposium (IPDPS). Presented at the 2019 IEEE International Parallel and Distributed Processing Symposium (IPDPS). Rio de Janeiro, Brazil: IEEE. pp. 314–324. doi:10.1109/IPDPS.2019.00041

Villeneuve AM, Hillers KJ. 2001. Whence meiosis? *Cell* **106**:647–650. doi:10.1016/s0092-8674(01)00500-1

Watanabe Y, Kitajima TS. 2005. Shugoshin protects cohesin complexes at centromeres. *Phil Trans R Soc B* **360**:515–521. doi:10.1098/rstb.2004.1607

Werner MS, Sieriebriennikov B, Prabh N, Loschko T, Lanz C, Sommer RJ. 2018. Young genes have distinct gene structure, epigenetic profiles, and transcriptional regulation. *Genome Res* **28**:1675–1687. doi:10.1101/gr.234872.118

Witte H, Moreno E, Rödelsperger C, Kim J, Kim J-S, Streit A, Sommer RJ. 2015. Gene inactivation using the CRISPR/Cas9 system in the nematode Pristionchus pacificus. *Dev Genes Evol* **225**:55–62. doi:10.1007/s00427-014-0486-8

Yoshida K, Kondoh G, Matsuda Y, Habu T, Nishimune Y, Morita T. 1998. The Mouse RecA -like Gene Dmc1 Is Required for Homologous Chromosome Synapsis during Meiosis. *Molecular Cell* **1**:707–718. doi:10.1016/S1097-2765(00)80070-2

Yu Z, Kim Y, Dernburg AF. 2016. Meiotic recombination and the crossover assurance checkpoint in Caenorhabditis elegans. *Seminars in Cell & Developmental Biology* **54**:106–116. doi:10.1016/j.semcdb.2016.03.014

Zhang C, Rabiee M, Sayyari E, Mirarab S. 2018. ASTRAL-III: polynomial time species tree reconstruction from partially resolved gene trees. *BMC Bioinformatics* **19**:153. doi:10.1186/s12859-018-2129-y

Zickler D, Kleckner N. 2015. Recombination, Pairing, and Synapsis of Homologs during Meiosis. *Cold Spring Harb Perspect Biol* **7**:a016626. doi:10.1101/cshperspect.a016626

Zickler D, Kleckner N. 1999. Meiotic Chromosomes: Integrating Structure and Function. *Annu Rev Genet* **33**:603–754. doi:10.1146/annurev.genet.33.1.603

Figure 1

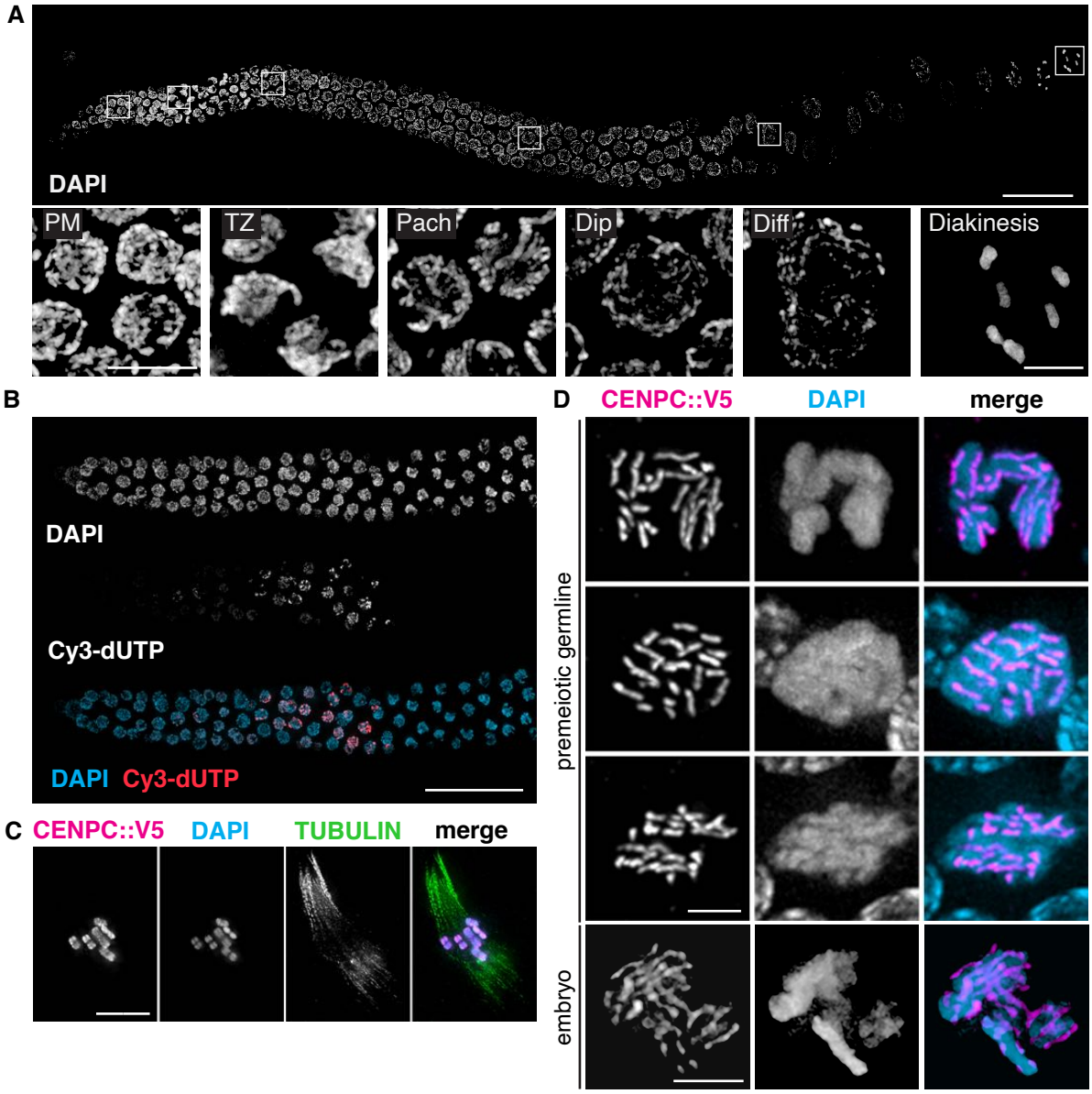
A
DAPI
PM
TZ
Pach
Dip
Diff
Diakinesis
B
DAPI
Cy3-dUTP
DAPI Cy3-dUTP
C CENPC::V5 DAPI TUBULIN merge
D CENPC::V5 DAPI merge
premeiotic germline
embryo

Figure 2

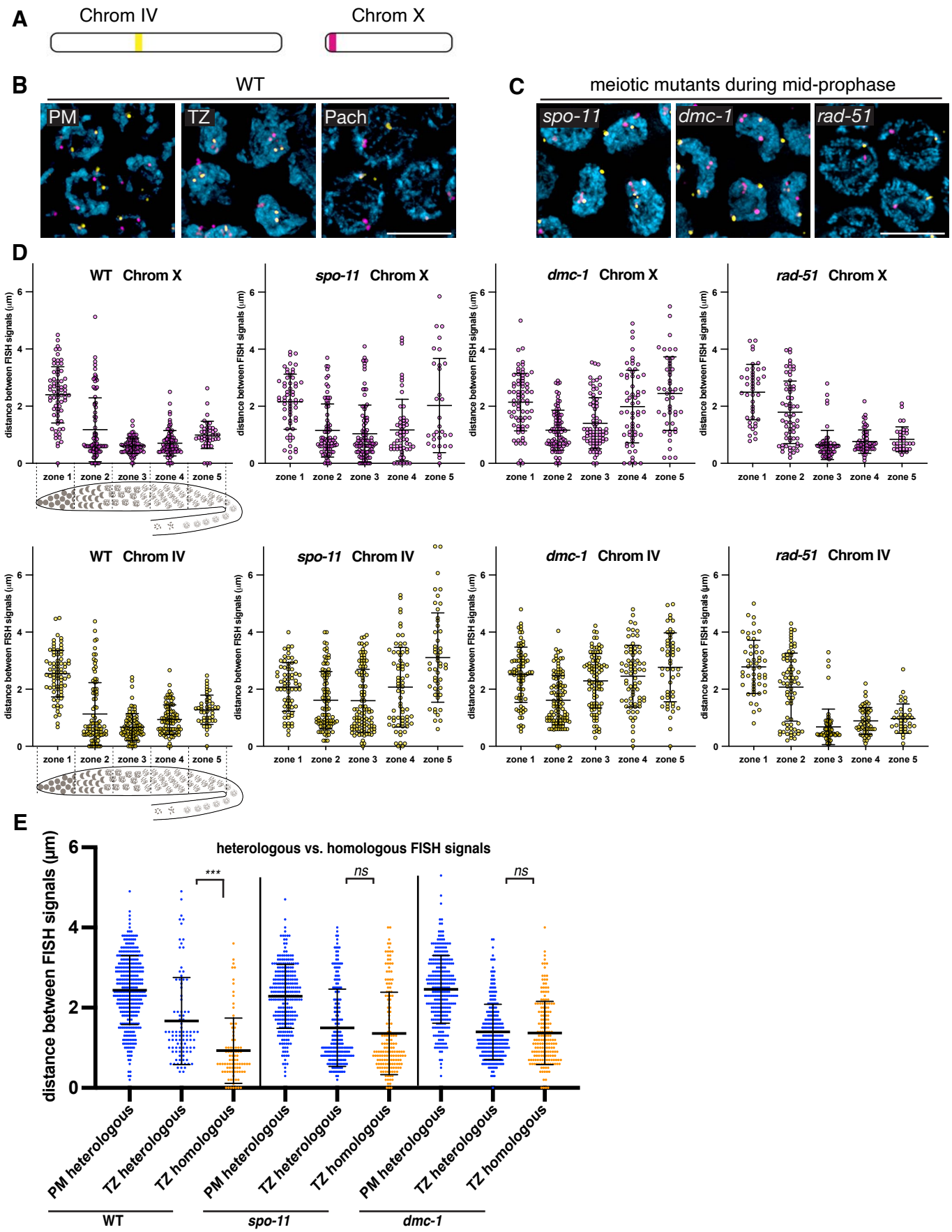
A
Chrom IV
Chrom X
B
WT
PM
TZ
Pach
C
meiotic mutants during mid-prophase
spo-11
dmc-1
rad-51
D
WT Chrom X
spo-11 Chrom X
dmc-1 Chrom X
rad-51 Chrom X
WT Chrom IV
spo-11 Chrom IV
dmc-1 Chrom IV
rad-51 Chrom IV
distance between FISH signals (µm)
zone 1
zone 2
zone 3
zone 4
zone 5
E
heterologous vs. homologous FISH signals
distance between FISH signals (µm)
***
ns
ns
PM heterologous
TZ heterologous
TZ homologous
WT
spo-11
dmc-1

Figure 2 - figure supplement 1

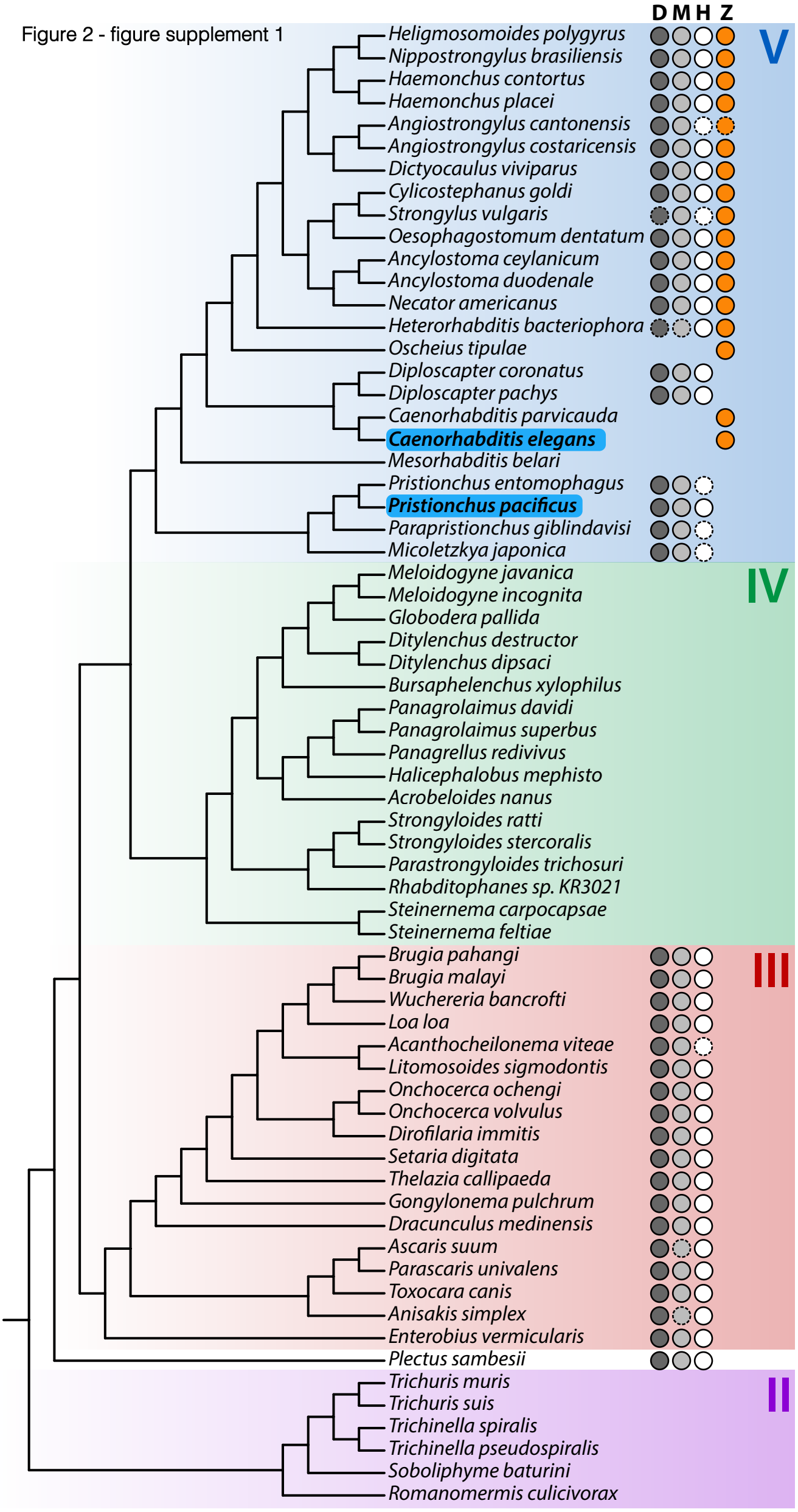

Figure 2- figure supplement 2

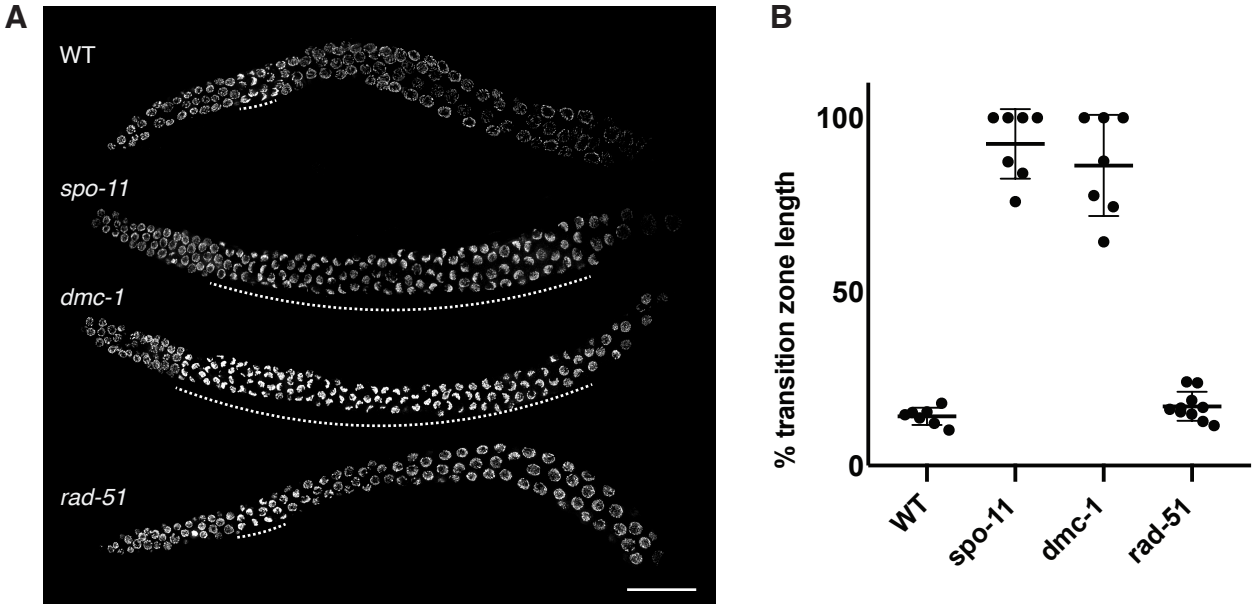

Figure 3

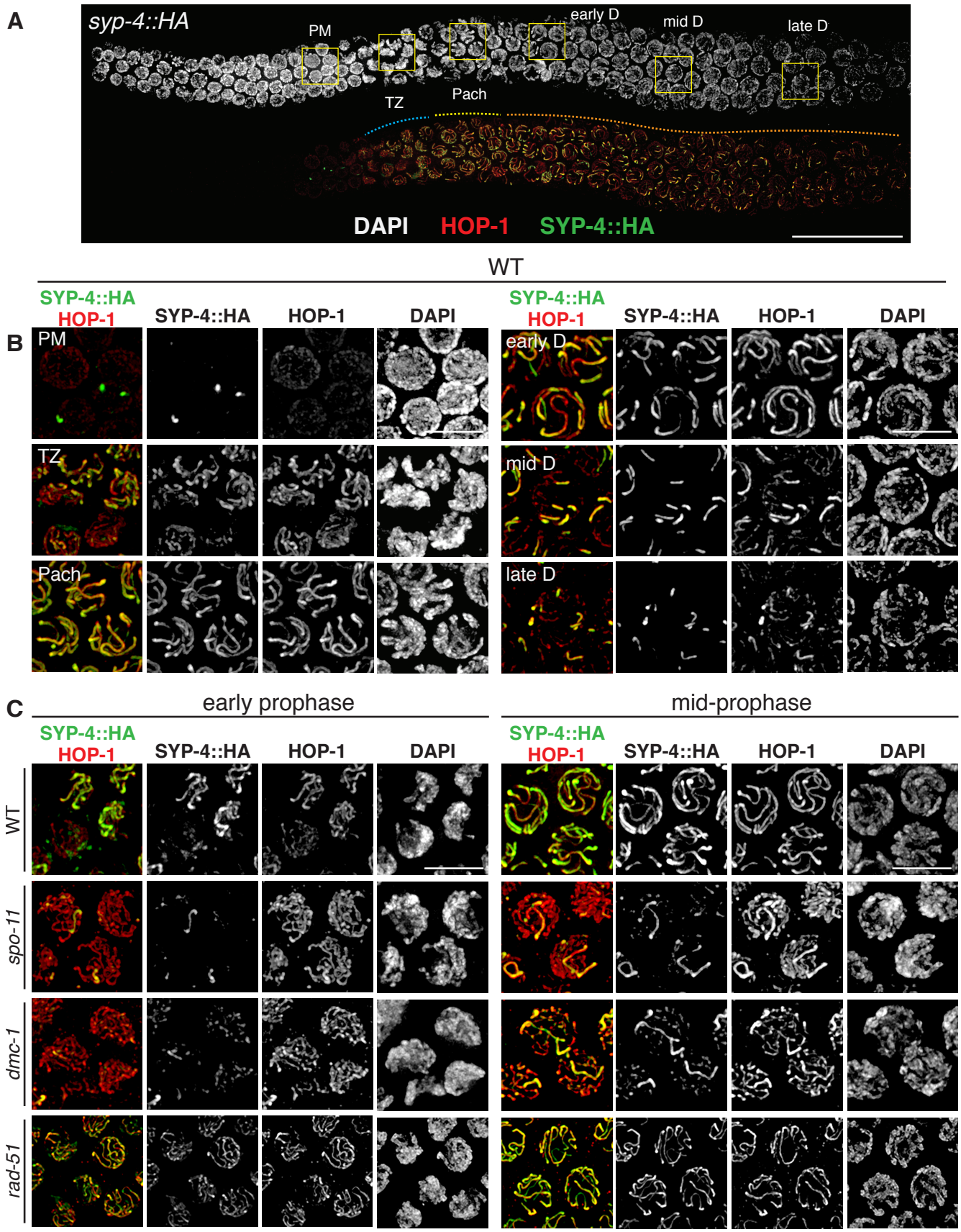
A
syp-4::HA
PM
TZ
Pach
early D
mid D
late D
DAPI
HOP-1
SYP-4::HA
WT
B
SYP-4::HA
HOP-1
SYP-4::HA
HOP-1
DAPI
PM
TZ
Pach
early D
mid D
late D
C
early prophase
mid-prophase
WT
spo-11
dmc-1
rad-51

Figure 3- figure supplement 1

Genotype	% Egg viability (±SD)	% Male progeny (±SD)	Eggs laid (± SD)
WT (n=30)	92.9 (±16.3)	0.9 (±1.0)	205 (±55)
syp-4::HA (n=7)	97.7 (±11.0)	0.5 (±0.6)	164 (±15)
dmc-1::V5 (n=8)	95.3 (±4.7)	1.1 (±1.4)	170 (±14)
rad-51::V5 (n=8)	107.1 (±18.9)	1.1 (±1.5)	157(±15)
syp-4::HA; dmc-1::V5; cosa-1::3xFLAG (n=8)	87.0 (±10.6)	0.4 (±0.6)	170 (±37)

Figure 4

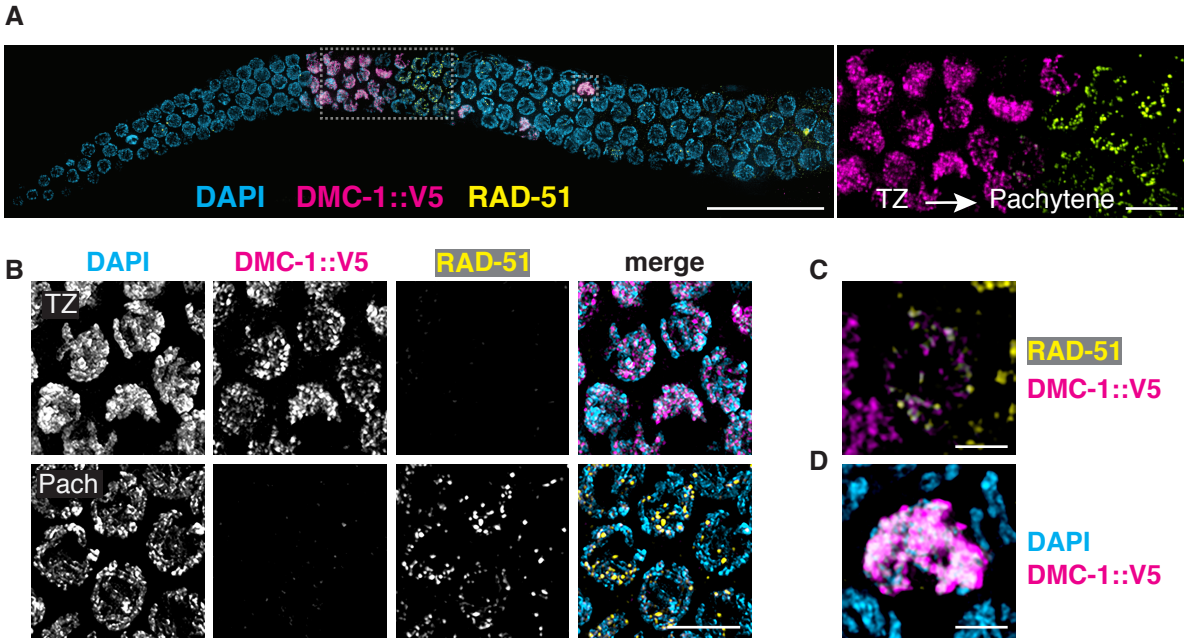
A
DAPI
DMC-1::V5
RAD-51
TZ
Pachytene
B
DAPI
DMC-1::V5
RAD-51
merge
TZ
Pach
C
RAD-51
DMC-1::V5
D
DAPI
DMC-1::V5

Figure 4- figure supplement 1

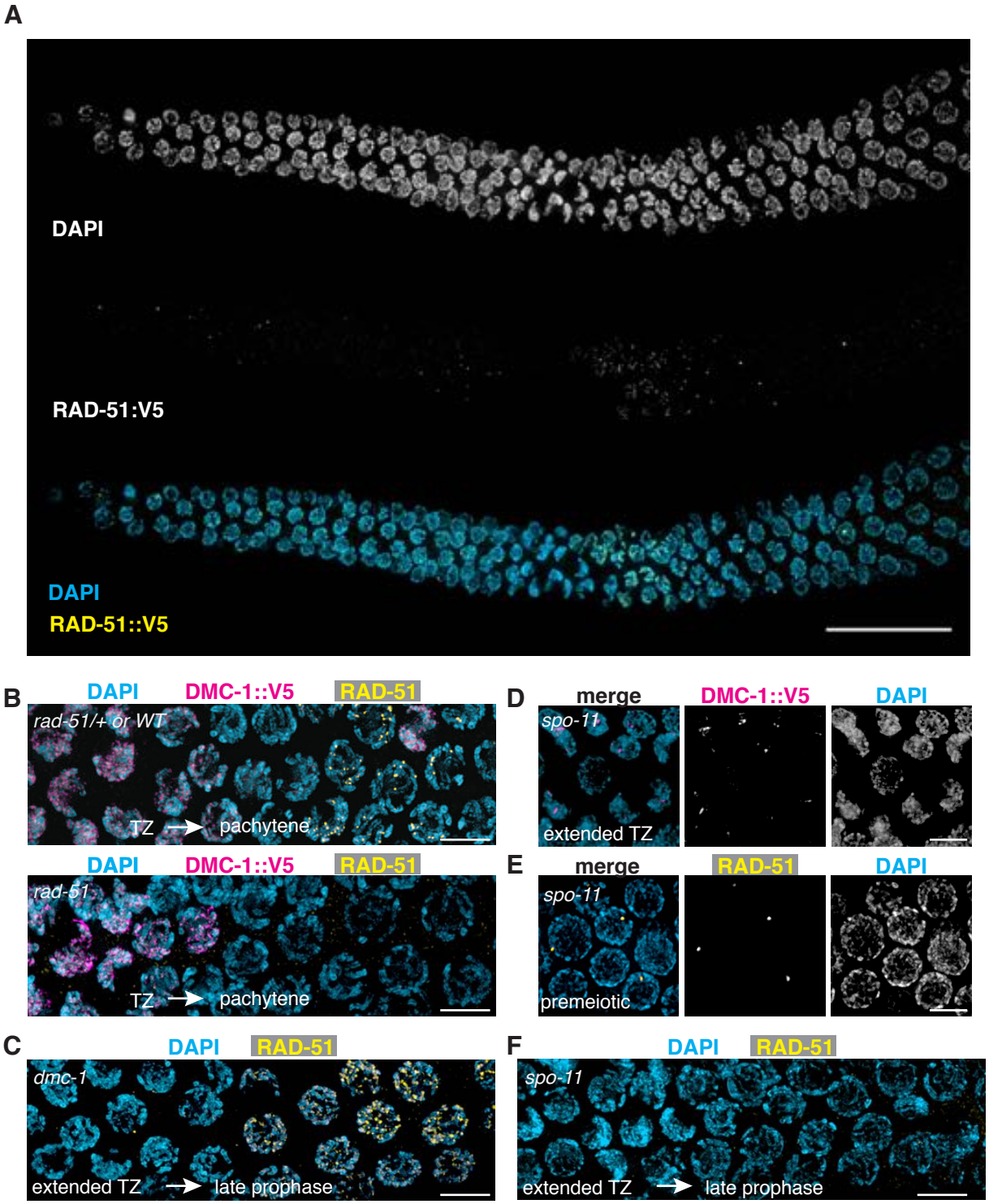

Figure 5

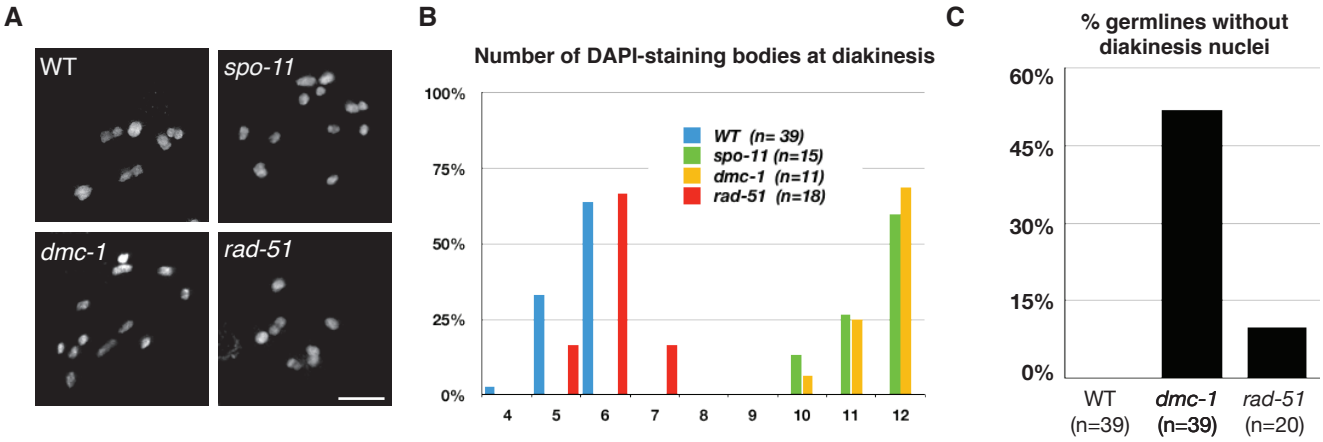

D

Genotype	% Egg viability (±SD)	% Male progeny (±SD)	Eggs laid (± SD)
WT (n=30)	92.9 (±16.3)	0.9 (±1.0)	205 (±55)
spo-11 (n=5)	0.3 (± .4)	20 (±44.7)	125 (±40)
dmc-1 (n=7)	0 (±0)	N/A	12 (±12)
rad-51 (n=14)	15.0 (±17.9)	4.5 (±5.1)	121 (±70)

Figure 6

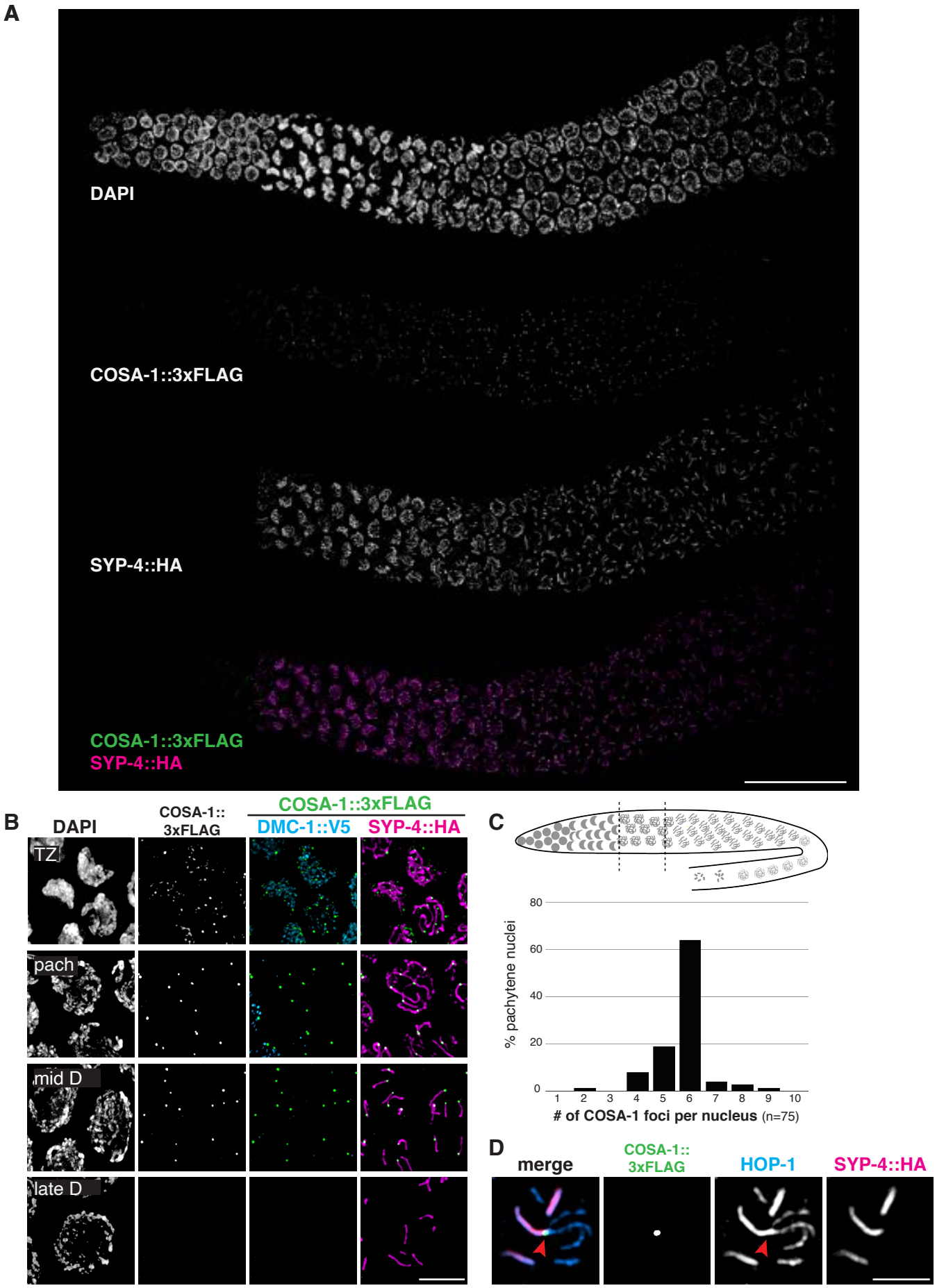
A
DAPI
COSA-1::3xFLAG
SYP-4::HA
COSA-1::3xFLAG
SYP-4::HA
B
DAPI
COSA-1::
3xFLAG
COSA-1::3xFLAG
DMC-1::V5
SYP-4::HA
TZ
pach
mid D
late D
C
% pachytene nuclei
80
60
40
20
0
1
2
3
4
5
6
7
8
9
10
# of COSA-1 foci per nucleus (n=75)
D
merge
COSA-1::
3xFLAG
HOP-1
SYP-4::HA

Figure 6- figure supplement 1

A

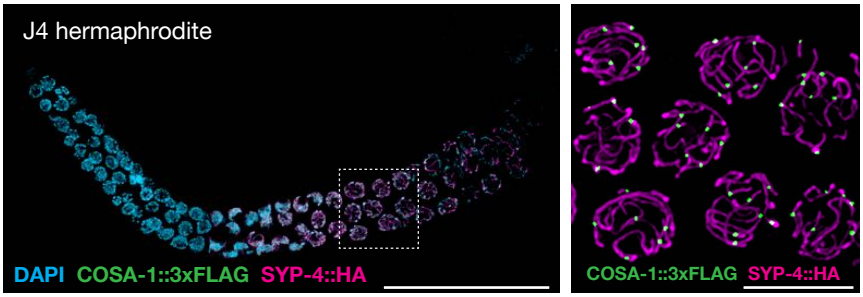

Figure 6- figure supplement 2

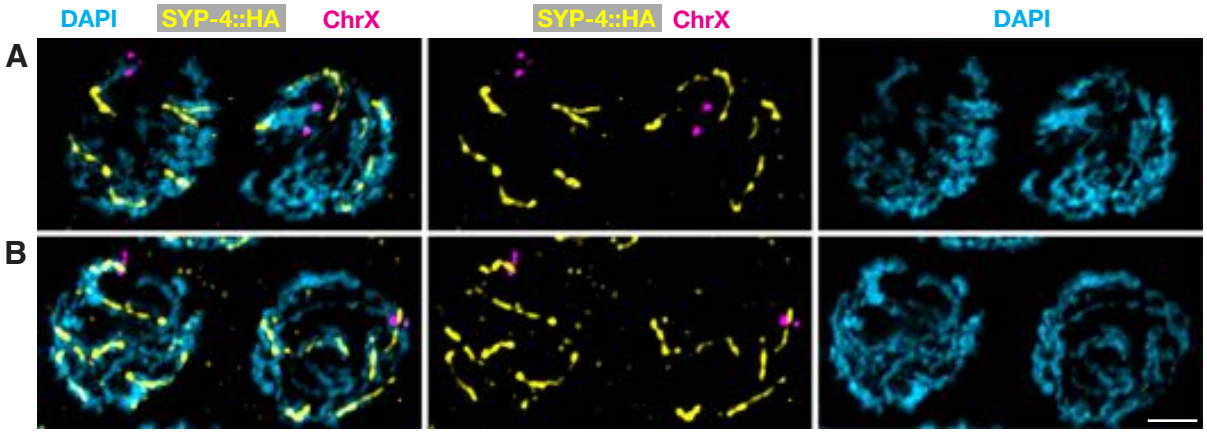

Figure 7

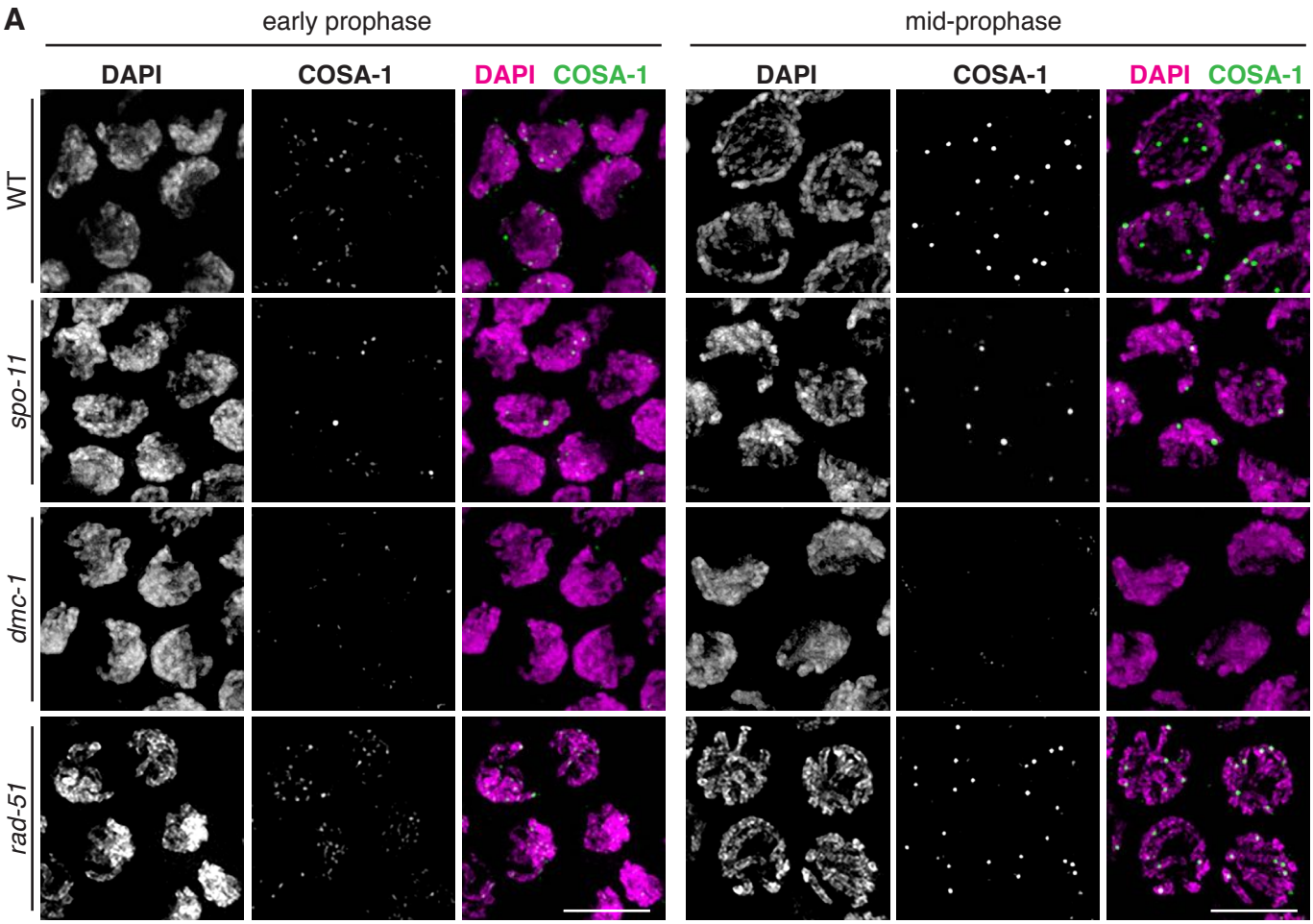
A
early prophase
mid-prophase
DAPI
COSA-1
DAPI COSA-1
DAPI
COSA-1
DAPI COSA-1
WT
spo-11
dmc-1
rad-51

Figure 8

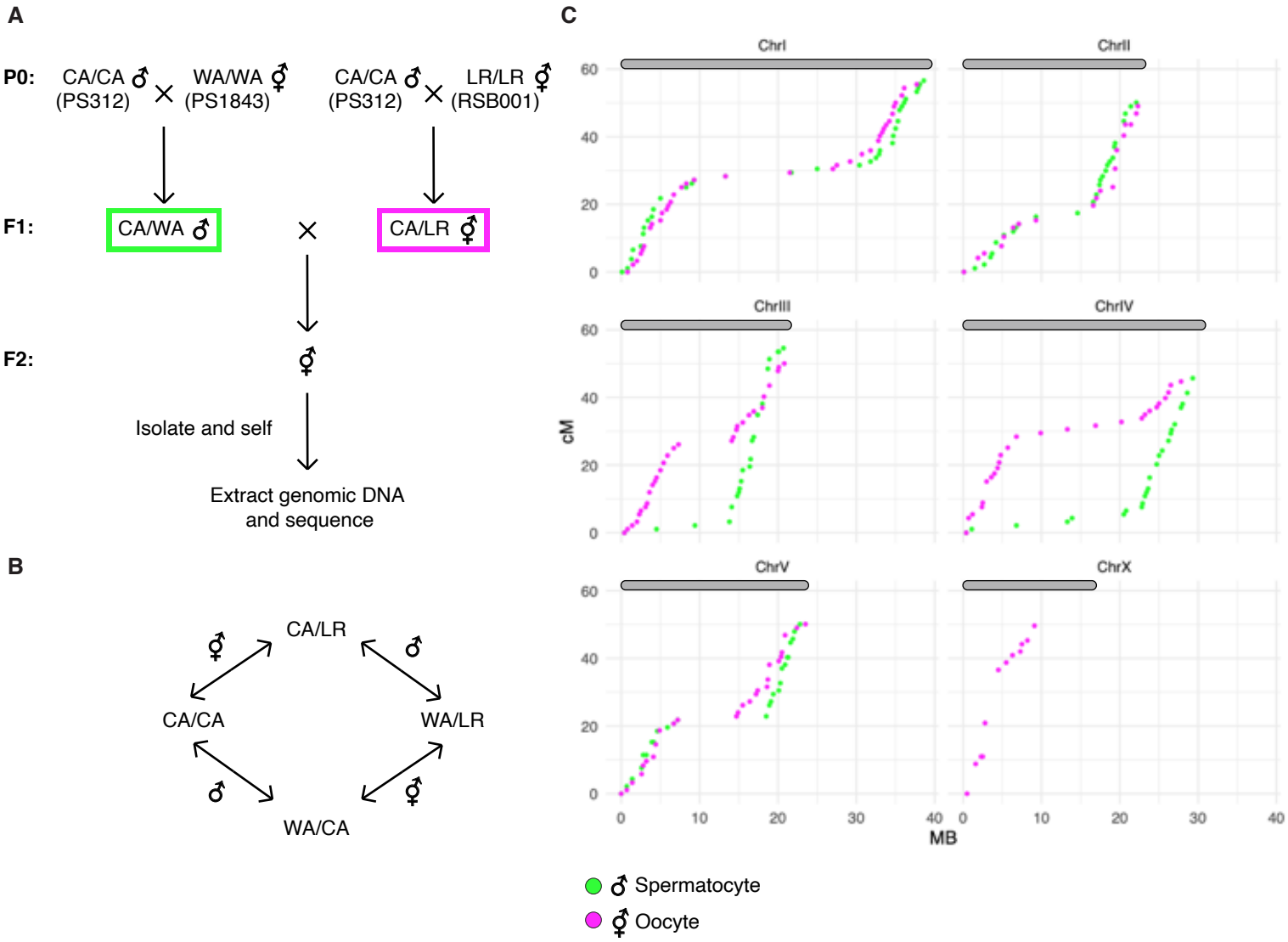
A
P0:
CA/CA ♂ (PS312)
WA/WA ⚥ (PS1843)
CA/CA ♂ (PS312)
LR/LR ⚥ (RSB001)
F1:
CA/WA ♂
CA/LR ⚥
F2:
⚥
Isolate and self
Extract genomic DNA and sequence
B
CA/LR
CA/CA
WA/LR
WA/CA
C
ChrI
ChrII
ChrIII
ChrIV
ChrV
ChrX
cM
MB
♂ Spermatocyte
⚥ Oocyte

Figure 8 - figure supplement 1

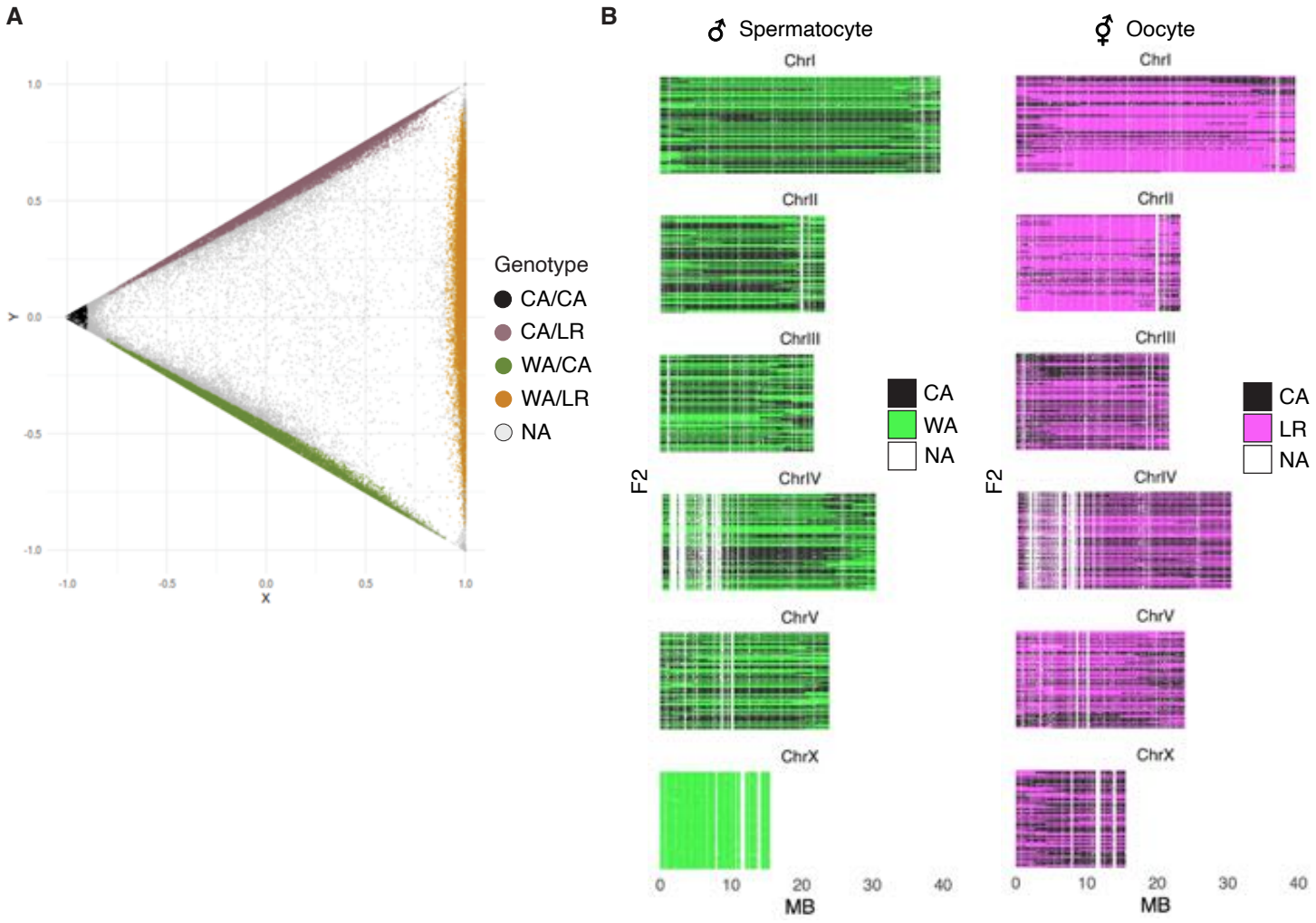

Table S1

Strain	El Paco genome reference, v1, 2017	Wormbase designation	Allele	Guide RNA target sequence (PAM sequence underlined)	ssDNA template	Genotyping primer sequences
cenpc::V5	*UMM-S71-6.7mRNA-1*	*PPA37734*	*ie1007*	ATGAAGAGATGGATTATAGTAGG	GGATATTAAAAAAAGGGGGTAAAATTGTACATCGCAAAAGGATGAGGAGTCATTTAATTCATCTTACTATAATCCATCTCTTCAGGTGGAGTCGAGTCCAAGAAGTGGGTTTGGAATTGGCTTTCCAGATCCGGCTCCTTCATTCTCTTCATCGAACTCTTCCACTTCCTTCTCCTTCTGCTCTTTTCTCTTCTTGTT	(f)TTTCTCCAGGAGTGGTTATCG (r)ACATCGCAAAAGGATGAGGAG
cosa-1::3xflag	*UMM-S57-3.22mRNA-1*	*PPA23791*	*ie1003*	CTTTATTCTTCATTTTACAGTGG	GATCATCCCAGGGAGAGAACGACCTACCCAAACAGAGATCATAGATCTAATTATCCACTGGGAGCCGGATCTGATTATAAAGACCATGATGGAGACTATAAGGATCACGATATTGATTACAAAGACGATGATGATAAATAAAATGAAGAATAAAGAGTATTAAATTTATGTTTGTGTTCGTTTTTGTAATTACTGCTTTG	(f)ACGACCTACCCAAACAGAGA (r)CGGATGTGGAAAGACGTACC
dmc-1 mutant	*UMM-S442-1.74mRNA-1*	—	*ie1005*	TTCGATAAGCTGCTTGGAGGTGG	ATTTAATTGTAACATTCAGACATCCAGTTGATCAACTAACCTCCGTTATTGCCTGACTTTCGATTCCACCactagtgTCCAAGCAGCTTATCGAATTCAACACTTCCAGTGGAGATTTTAAAGACTTGCTTGCGTCGTGAACACACT	(f)GGACTCTCGGAGGCTAAAGT (r)ATTCTCGAGCATTGCTTCCT
dmc-1::V5	*UMM-S442-1.74mRNA-1*	—	*ie1001*	GCAACGTTTGCCATTGCAGCAGG	GATAAAACATGATCTTTTGTCCTTCATAATTGATTAGGTGGAGTCGAGTCCAAGAAGTGGGTTTGGAATTGGCTTTCCATCCTTTGCATCGACAATTCCTCCTGC**G**GC**G**ATGGCAAACGTTGCTTCGTTCTCAGGCATATC	(f)TGCCTGAGAACGAAGCAACG (r)ACATGAGATGGCACAAAGGAC
hop-1	*UMM-S341-6.31mRNA-1*	*PPA10281*				
rad-51 mutant	*UMM-S442-1.74mRNA-1*	*PPA42255*	*ie1006*	GTCGAGAACGAGGAGAATGCCGG	ATTTATTGGTTACCTCAAGGGACATGATGGACTGGCAGGCGAGTCCGGCATACTAGTTTCTCCTCGTTCTCGACATCAGCGTCGACGTGCGCCATTTGAGCGGACAT	(f)TTCTAGTGACGCGTGTTGTT (r)ACGAATCCTCGTTGCTGAAG

rad-51::V5	*UMM-S442-1.74mRNA-1*	*PPA42255*	*ie1008*	GACCTTCTCCATCACAACAA CGG	GATGGTCAGATAACAGCTATGGAGTGTGTAAATTG GAGAGAGTTAGACGACTAGGTGGAGTCGAGTCCA AGAAGTGGGTTTGGAATTGGCTTTCCATTATCCTTT CCATCTTCGATGCCCGTGGTGGTGATGGAGAAGG TCGCCTCGCCCTCGGCCAGGCATGGAGATTG	(f)GATTCATCTCTGTTTCACAG G (r)GATCTCGGTTTCTCTCTTGG AAA
spo-11 mutant	*UMM-S230-10.9mRNA-1*	*PPA33054*	*ie1004*	ATTCAGAACTTGGCAGAGAT CGG	ACAAACATCTTTTTGCACGACAGGATTCTCTCAA TCGATCAGTTTCCGATAACTAGTACTCTGCCAAGTT CTGAATATGCAAAGATGTCAAGTCAATGTGGTAA GT	(f)GGAAATCCTTCGTTCTCACT ATGG (r)GTCTCAATATCAGACAATTT CATTCCG
syp-4::HA	*UMM-S245-8.16mRNA-1*	—	*ie1002*	GGAGGAGAATTCAACTTCTT CGG	CAAATGGAGGTGGCGGCGGGGGAGGAGGAGA GTTTAATTTTTTTGGTTTTTACCCCTACGATGTCC CAGATTATGCTTAAACCAATTTTTTCGAGCTTGGT GTAATGTATCCA	(f)CCCGTTGATGATGCTACCA G (r)GATACATTACACCAAGCTC GAA

Table S2

Species	Accession	Version	Source
Acanthocheilonema viteae	PRJEB1697	WBPS15	WormBase ParaSite
Acrobeloides nanus	PRJEB26554	WBPS15	WormBase ParaSite
Ancylostoma ceylanicum	PRJNA231479	WBPS15	WormBase ParaSite
Ancylostoma duodenale	PRJNA72581	WBPS15	WormBase ParaSite
Angiostrongylus cantonensis	PRJNA350391	WBPS15	WormBase ParaSite
Angiostrongylus costaricensis	PRJEB494	WBPS15	WormBase ParaSite
Anisakis simplex	PRJEB496	WBPS15	WormBase ParaSite
Ascaris suum	PRJNA62057	WBPS15	WormBase ParaSite
Brugia malayi	PRJNA10729	WBPS15	WormBase ParaSite
Brugia pahangi	PRJEB497	WBPS15	WormBase ParaSite
Bursaphelenchus xylophilus	PRJEA64437	WBPS15	WormBase ParaSite
Caenorhabditis elegans	PRJNA13758	WBPS15	WormBase ParaSite
Caenorhabditis parvicauda	PRJEB12595	WBPS15	WormBase ParaSite
Cylicostephanus goldi	PRJEB498	WBPS15	WormBase ParaSite
Dictyocaulus viviparus	PRJNA72587	WBPS15	WormBase ParaSite
Diploscapter coronatus	PRJDB3143	WBPS15	WormBase ParaSite
Diploscapter pachys	PRJNA280107	WBPS15	WormBase ParaSite
Dirofilaria immitis	PRJEB1797	WBPS15	WormBase ParaSite
Ditylenchus destructor	PRJNA312427	WBPS15	WormBase ParaSite
Ditylenchus dipsaci	PRJNA498219	WBPS15	WormBase ParaSite
Dracunculus medinensis	PRJEB500	WBPS15	WormBase ParaSite
Enterobius vermicularis	PRJEB503	WBPS15	WormBase ParaSite
Globodera pallida	PRJEB123	WBPS15	WormBase ParaSite
Gongylonema pulchrum	PRJEB505	WBPS15	WormBase ParaSite
Haemonchus contortus	PRJEB506	WBPS15	WormBase ParaSite
Haemonchus placei	PRJEB509	WBPS15	WormBase ParaSite
Halicephalobus mephisto	PRJNA528747	WBPS15	WormBase ParaSite
Heligmosomoides polygyrus	PRJEB15396	WBPS15	WormBase ParaSite
Heterorhabditis bacteriophora	PRJNA13977	WBPS15	WormBase ParaSite
Hypsibius dujardini	-	3.1.5	tardigrades.org
Litomosoides sigmodontis	PRJEB3075	WBPS15	WormBase ParaSite
Loa loa	PRJNA246086	WBPS15	WormBase ParaSite
Meloidogyne incognita	PRJNA340324	WBPS15	WormBase ParaSite
Meloidogyne javanica	PRJNA340324	WBPS15	WormBase ParaSite
Mesorhabditis belari	PRJEB30104	WBPS15	WormBase ParaSite
Micoletzkya japonica	PRJEB27334	WBPS15	WormBase ParaSite
Necator americanus	PRJNA72135	WBPS15	WormBase ParaSite
Nippostrongylus brasiliensis	PRJEB511	WBPS15	WormBase ParaSite
Oesophagostomum dentatum	PRJNA72579	WBPS15	WormBase ParaSite
Onchocerca ochengi	PRJEB1204	WBPS15	WormBase ParaSite
Onchocerca volvulus	PRJEB513	WBPS15	WormBase ParaSite
Oscheius tipulae	PRJEB15512	WBPS15	WormBase ParaSite

Species	Accession	Version	Source
Panagrellus redivivus	PRJNA186477	WBPS15	WormBase ParaSite
Panagrolaimus davidi	PRJEB32708	WBPS15	WormBase ParaSite
Panagrolaimus superbus	PRJEB32708	WBPS15	WormBase ParaSite
Parapristionchus giblindavisi	PRJEB27334	WBPS15	WormBase ParaSite
Parascaris univalens	PRJNA386823	WBPS15	WormBase ParaSite
Parastrongyloides trichosuri	PRJEB515	WBPS15	WormBase ParaSite
Plectus sambesii	PRJNA390260	WBPS15	WormBase ParaSite
Pristionchus entomophagus	PRJEB27334	WBPS15	WormBase ParaSite
Pristionchus exspectatus	PRJEB24288	WBPS15	WormBase ParaSite
Ramazzottius varieornatus	-	Rv101	tardigrades.org
Rhabditophanes kr3021	PRJEB1297	WBPS15	WormBase ParaSite
Romanomermis culicivorax	PRJEB1358	WBPS15	WormBase ParaSite
Setaria digitata	PRJNA479729	WBPS15	WormBase ParaSite
Soboliphyme baturini	PRJEB516	WBPS15	WormBase ParaSite
Steinernema carpocapsae	PRJNA202318	WBPS15	WormBase ParaSite
Steinernema feltiae	PRJNA204661	WBPS15	WormBase ParaSite
Strongyloides ratti	PRJEB125	WBPS15	WormBase ParaSite
Strongyloides stercoralis	PRJEB528	WBPS15	WormBase ParaSite
Strongylus vulgaris	PRJEB531	WBPS15	WormBase ParaSite
Thelazia callipaeda	PRJEB1205	WBPS15	WormBase ParaSite
Toxocara canis	PRJNA248777	WBPS15	WormBase ParaSite
Trichinella pseudospiralis	PRJNA257433	WBPS15	WormBase ParaSite
Trichinella spiralis	PRJNA12603	WBPS15	WormBase ParaSite
Trichuris muris	PRJEB126	WBPS15	WormBase ParaSite
Trichuris suis	PRJNA179528	WBPS15	WormBase ParaSite
Wuchereria bancrofti	PRJNA275548	WBPS15	WormBase ParaSite

Table S3

SSLP marker	Chromosome	Primer sequences
L2	I	(f)GGAATGAGGGTCGTGAGGTA (r)GCGTTTTCAAAATGAAGCAA
L23	III	(f)AATTCGCAATGACCTATGAGA (r)ACAAATTCGTCACTCTGGCA
L109	III	(f)GTCCACCGTACCTCTCACCT (r)TCTTGATCCATCGGAATGCT
L100	IV	(f)CGATCGCCGTTTACGAGG (r)GTCCCGCATAGCAACCAATA
L106	IV	(f)GAAAGGGACTGCGGAACTC (r)GTACAGCGTACCGTCCGATT
L16	V	(f)TGAACACTTTCAATGCCTCTTT (r)GTCGATCTTGATCTTGTCCG

Table S4

Software	***Version***	***Relevant parameters***
catfasta2phyml	-	-c -f
edgeR	3.18.0	
HTSeq	0.6.1	
IQ-TREE	1.6.10	-bb 1000, -bb -m GTR20+G
MAFFT	7.407	--auto
NCBI-BLAST+	2.5.0+	blastp
OrthoFinder	2.2.7	-og
PhyloTreePruner	20150918	35 0.9 u
Priism	4.7.1	
R	3.5.1	
softWorx	7.0.0	
STAR	2.5.2	--outFilterType BySJout --outFilterMultimapNmax 20 --alignSJoverhangMin 8 -alignSJDBoverhangMin 8 --outFilterMismatchNmax 999 --outFilterMismatchNoverReadLmax 0.04 --alignIntronMin 20 --alignIntronMax 1000000 --alignMatesGapMax 1000000
StringTie	1.3.3	-p 10 -m 50 --rf -f 0.1 -a 10 -j 5 -c 2.5
Transdecorder	3.0.1	
trimalAl	v1.4.rev15	-gt 0.8 -st 0.001 -resoverlap 0.75 -seqoverlap 80